IDCOR

Program Report

DRAFT

Technical Report

RESUSPENSION OF DEPOSITED AEROSOLS
FOLLOWING PRIMARY SYSTEM OR
CONTAINMENT FAILURE

RESUSPENSION OF DEPOSITED AEROSOLS FOLLOWING PRIMARY SYSTEM OR CONTAINMENT FAILURE

July, 1984

TABLE OF CONTENTS

TABLE OF CONTENTS (Continued)

LIST OF FIGURES

LIST OF TABLES

ABSTRACT

A postulated, severe degraded core accident may result in failure of the reactor vessel and the release of radioactive aerosol particles to the containment building. Deposition of particles within the primary system and on the walls, floors and water pools of the containment will contribute to the decontamination of the containment atmosphere. This report first critically examines available laboratory data on the adhesion and removal of particles from solid surfaces by tangential flows. Next the fundamental models are applied to the general accident behavior to assess the extent of resuspension of deposited aerosol particles in the event of containment failure. Thirdly, the potential for resuspension by dispersing a layer of accumulated material is examined analytically and experimentally. Lastly, these results are extended to the reactor primary system and containment designs analyzed in the IDCOR program. The basic conclusion for these analyses is that no significant amount of material would be resuspended following either reactor vessel failure or containment failure.

NOMENCLATURE

A	Area of surface sampled in particle resuspension experiments
A_F	Flow area through hot leg and cold leg piping
A_H	Area of containment failure hole
c	Particle concentration in containment atmosphere (g cm^{-3})
c_R	Particle concentration released to the containment atmosphere (g cm^{-3})
d	Particle diameter
D	Diameter of parallel-plate channel
f	Friction factor for turbulent flow (~ 0.005)
F	Particle adhesion force
K	Particle mass-transfer coefficient (cm s^{-1})
$\dot{m}$	"Choked" flow rate through containment failure hole (g s^{-1})
$\dot{m}''_d$	Particle deposition mass flux (g cm^{-2} s^{-1})
$\dot{m}''_r$	Particle resuspension mass flux (g cm^{-2} s^{-1})
M	Particle mass collected in particle resuspension experiments
P	Containment or reactor vessel gas pressure
q	Electrostatic charge
r	Radial distance from failure hole
r_H	Effective radius of failure hole
R	Ideal gas constant for containment gas
S	Containment surface area for particle deposition
t	Time
T	Containment gas temperature
u	Gas velocity in boundary layer or in particle bed
U	Gas velocity in
U_∞	Mainstream gas velocity and local containment gas velocity

U_s	Stokes velocity for levitating individual particles
U_t	Sonic gas velocity at failure hole
V	Volume of containment building
x	Closest distance from particle to surface
y	Transverse coordinate measured from channel wall into the boundary layer
z	Vertical coordinate measured from containment floor

Greek Symbols

β	London-Van der Waals constant of proportionality (ergs), see Eq. (2.2)
γ	Ratio of specific heats of containment gas
ε	Dielectric constant or particle bed porosity
κ	Permeability of particle bed
Λ	Resuspension rate parameter (s^{-1})
μ	Absolute viscosity of gas
ρ	Density of gas
ρ_a	Density of atmosphere outside containment
ρ_p	Density of particle material
ρ_t	Gas density at choking (sonic) location
σ	Surface tension of adsorbed film
ν	Kinematic viscosity of gas
χ	Surface concentration of deposited aerosol particles (g cm^{-2})
η	Isothermal critical pressure ratio

Subscript

o	Refers to conditions in containment or in the vessel at the instant of failure

1.0 INTRODUCTION

A consideration of the potential for resuspension of deposited, radioactive aerosol particles as a result of both reactor vessel failure and containment failure is presented in this report. In particular, the nature of the interaction of adhering, dry particulate on vertical and horizontal structural surfaces produced by the depressurization through the failure location is examined. In particular, resuspension as a result of entrainment due to tangential flows and dispersion due to normal flows are considered and applied to general reactor accident conditions.

Aerosol particles, radioactive or not, will attach firmly to any surface they contact. This is one of the major characteristics that distinguishes them from gas molecules. In fact, all particle collection mechanisms which form the basis for the design of industrial and residential air cleaning apparatus rely on adhesion of particles. The adhesive forces between particles less than 10 μm in thin layers and the substrate exceeds other common forces, such as gravity and forces produced by air currents, by orders of magnitude.

It is important to note that at present there is not a satisfactory procedure for reliably predicting these forces from the physical and chemical properties of the particles and substrate materials. However, present empirical knowledge does enable us to understand the nature of the forces involved, as well as the variables influencing their strength. In addition, we can calculate both the order of magnitude of these forces and the rate of particle removal and conclude that the potential for significant resuspension due to tangential flows (or "re-entrainment") of radioactive particles in a failed containment building is very small.

The forces associated with dispersion of accumulated layers can be characterized in terms of a basic model. This model can be compared with laboratory data and also extrapolated to the reactor system to determine the potential for significant resuspension due to depressurization.

In general, the report addresses containment conditions since these are directly related to the atmospheric release fraction. However, the amount of material resuspended following reactor vessel failure is also a process to be critically examined. This is accomplished by first reviewing pertinent experimental results and fundamental models for resuspension by tangential flows. Next, the potential for resuspension dispersing accumulated layers is addressed through laboratory experiments and basic models. After the various mechanisms are presented and discussed, the results are extended to the primary system and containment conditions of interest.

2.0 ADHESION FORCES

Several workers have noted the marked adhesion between solid surfaces when liquid is present between the surfaces. Bowden and Tabor [1] have shown that the adhesion of a sphere to a plane surface with a small amount of interposed liquid between the two surfaces agrees with the theoretical value

$$F = 2\pi\sigma d \tag{2.1}$$

where F is the adhesion force perpendicular to the plane surface, σ is the surface tension of the interposed liquid and d is the diameter of the sphere. Under normal or "dry" conditions a contact liquid film may not be present on the plane surface or substrate. Nevertheless, most materials have adsorbed liquid (water) molecules on their surface, and there is an attractive force between particle and substrate because of the surface tension of the liquid drawn into the capillary space at the point of contact. Under these dry conditions, however, measured forces of adhesion of particles to plane surfaces in air are considerably lower than adhesion forces predicted by Eq. (2.1). The force of adhesion approaches the Eq. (2.1) value at relative humidities greater than 90%. At 80% relative humidity, for example, the force is reduced by a factor of two [1].

Another important adhesion force is the London-Van der Waals force, which arises because of the random movement of electrons in any material creates instantaneous areas of charge concentration. These charge concentrations induce complementary charge concentrations in neighboring material, which result in attractive forces. Hamaker [2] and Bradley [3] derived the following expression for the London-Van der Waals attractive force between a sphere of diameter d and a flat plate separated by a distance x:

$$F = \beta \frac{d}{x^2} \tag{2.2}$$

where β is a constant of proportionality that must be determined by experiment. Note that the London-Van der Waals force decreases rapidly with separation distance; its influence extends only over separation distances of several

molecular diameters. Careful experiments performed by Deryagin [4] and Prosser and Kitchener [5] indicate that $\beta \sim 10^{-12}$ erg. Clearly, in order to apply Eq. (2.2) to the adhesion of real particles it is necessary to make assumptions about the distance of approach of the surfaces, x. Since the distance x depends on the scale of the surface roughness, it is difficult to make accurate quantitative predictions of the London-Van der Waals force.

Kunkel [6] studied the electrification of particles from 1.0 to 72 μm size in particulate clouds of quartz, sulfer and rice starch. All aerosols dispersed by an air stream were found to be electrostatically charged, and contained both negatively and positively charged particles simultaneously. Qualitative laboratory studies by Berg and Brunetz [7] and Deryagin and Zimon [8] indicate that the adhesive bond between a particle and a substrate is increased when the net number of unit charges per particle increases. Presumably, if the charge is localized on the surface of the particle, it will induce a charge on the substrate surface which is equal and opposed to that it carries. If the particle carries a charge q and is separated a distance x from opposite charges by a dielectric medium ε, the induced electrical force on the particle will be

$$F = \frac{\varepsilon q^2}{x^2} \tag{2.3}$$

The equilibrium charge carried by particles larger than 0.1 μm is approximately proportional to $d^{1/2}$, so that the electrostatic adhesion force, like the surface tension and London-Van der Waals forces, is proportional to the first power of diameter. Unfortunately, Eq. (2.3) can only be loosely related to experimental measurements. While laboratory electrostatics [7-10] support the large role played by electrostatics in the adhesion of particles, Eq. (2.3) indicates that to cause the observed behavior the charges associated with particles would have to be very large and out of line with the average charges on particulates in aerosol clouds [6].

It can be concluded from the discussion in the foregoing that the calculation of adhesion forces of particles is approximate, at best. In air, where adhesion forces due to electrostatic charge and adsorbed moisture

content may be operating simultaneously, it is difficult to distinguish one adhesion mechanism from another or to determine which force may dominate. The difficulty in isolating adhesion forces is attested to, for example, by spurious effects due to static charge present in experiments for evaluating the Van der Waals constant β in Eq. (2.2) [11,12]. While the adhesive force relations covered here are of limited practical value, they do show that the strength of the bond between a particle and a substrate is proportional to the particle diameter. Indeed, this is the form of the empirical expressions for adhesive force.

Experimental measurements of adhesive forces are made by determining the force required to separate a particle from a surface. These may be direct measurements using a fiber microbalance or centrifugal force, or they may be indirect measurements using vibration or air flows to remove the particles.

Kordecki and Orr [13] made an extensive experimental study of the particle removal force in different particle-substrate systems. Glass, sand, charcoal and rubber particles of 50 μm diameter were used. The substrate materials included metals, brick, enamel (painted material), glass and wood. The force required to remove 98% of the particles from the substrates varied from 0.3 to 10 dynes, depending on the material pair and the prevailing relative humidity. Static charge must have been present during these measurements since the forces of adhesion were higher at 10% or 50% relative humidity than at 90% relative humidity. It is well known that insulating materials at low humidities retain their charge.

Corn [14] used a microbalance to study the influence of particle size on adhesion force. He found the force of adhesion between quartz or Pyrex particles and a Pyrex substrate in air at 90% relative humidity to be given by $F \approx 0.015\ d$, where F is in dynes and d is the particle diameter in microns. Boehm et al. [15] showed that 13-15 μm starch particles were removed with forces from 0.1-1.4 dyne. Apparently there is a dependence of adhesion on particle size, but there is also a large scatter of adhesive force about any one particle size. A useful expression for the adhesive force that represents a lower bound to the measurements is given by

$$F = 0.0006\ d \qquad (2.4)$$

where the force is in dynes and the particle diameter is in microns.

Equation (2.4) is based on direct measurement at 300°K. This is below the temperature range of interest in fission product transport within containment. Temperature could influence the adhesive force by altering the surface tension of the adsorbed surface film or by removing ("drying") the adsorbed film. Interestingly enough, relatively recent laboratory measurements by Bhattacharya and Mittal [16] show that the heating of adhering particles to temperatures well above the boiling temperature of the adsorbed film material actually results in increased particle adherence. Even in the absence of the capillary force the "dry" adhesive forces, London-Van der Waals and electrostatic, should be unaffected by high temperatures, and order of magnitude estimates using Eqs. (2.2) and (2.3) indicate that the majority of particles should still be held with forces of the order of that predicted by Eq. (2.4). In actual fact, the force of adhesion is observed to increase with temperature due to the "softening" of the contact zone between the particle and the surface. Polke [17] reported on the adhesion of gold particles to various surfaces over a range of temperatures from 300 to 673°K. The adhesion force was found to increase with increasing temperature, and a value of 50 dynes was measured at 673°K, which is three orders of magnitude greater than the force calculated from Eq. (2.4). The adhesive force between glass particles and painted surfaces shows a dramatic increase with increasing surface temperature [18]. The greater adhesion to painted surfaces at high temperature is simply explained as a result of surface tack. This is an important finding as the majority of the structural surfaces in the containment building are painted.

Figure 2.1 shows some experimental data on the adhesion of particles in various particle-substrate systems. The measurements were made using either a microbalance or a centrifuge. The results show that there is a large variation in the adhesion of the same size particle in different particle-substrate systems. It is clear from the figure that the adhesive forces exceed the force due to gravity by orders of magnitude. Also, the measured forces exceed the prediction of Eq. (2.4) by more than an order of magnitude.

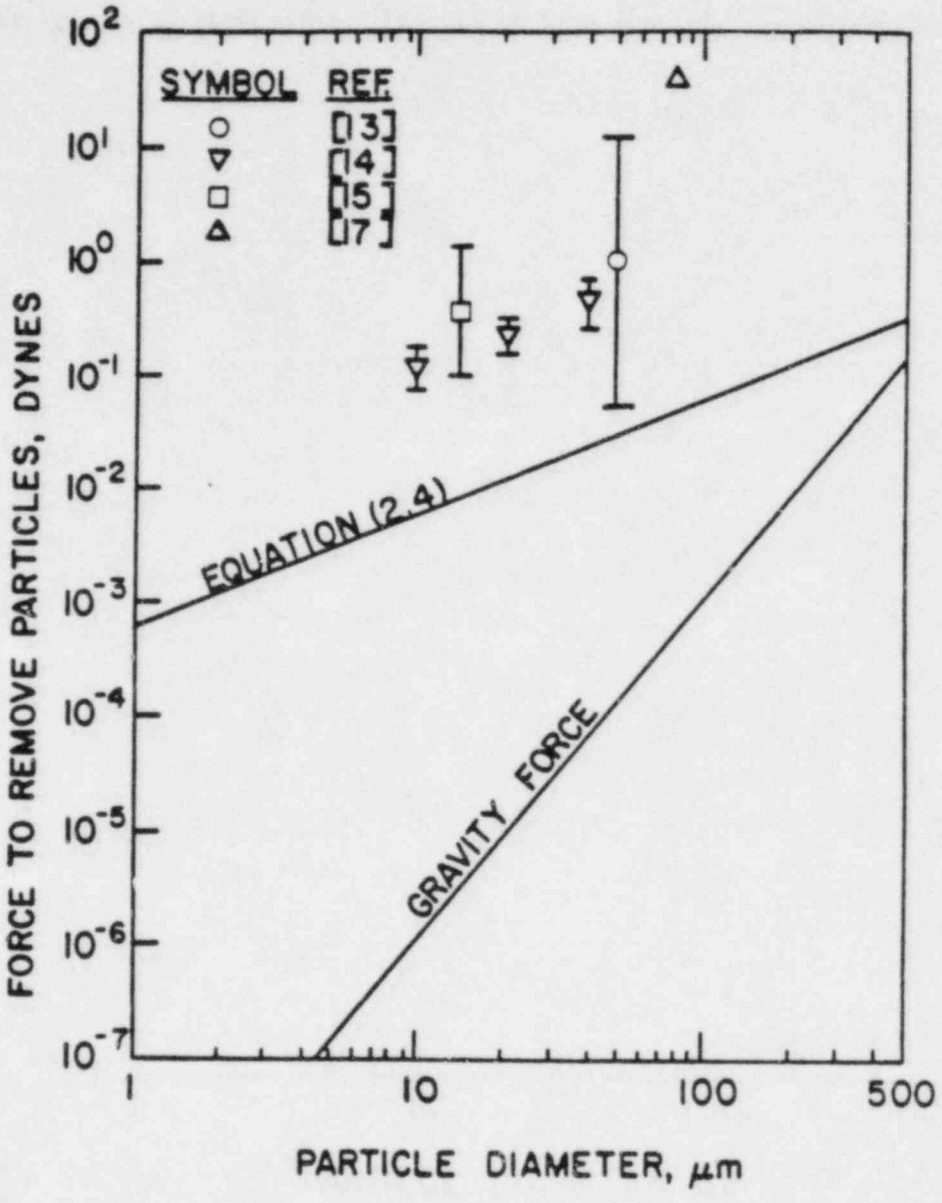

Fig. 2.1 Measured force of adhesion as a function of particle diameter. The force exerted by gravity on particles of specific gravity 2.0 is shown for comparison.

The discussion in the foregoing is a summary of the work or the adhesion of individual particles to solid substrates. It should be noted that particles that exist in layers are also subject to cohesive forces (between particles) which could be as important as the adhesive forces between the particles and the surface.

3.0 PARTICLE RESUSPENSION IN GAS FLOW

The problem of particle removal by fluid flow has received a moderate amount of attention during the past 40 years and the experimental data which exists is largely concerned with the entrainment and transportation of relatively large particles in air and river bed flows. A convenient summary of work in this area is presented by Raudviki [19]. Another class of problem associated with the cleaning of soiled surfaces is concerned with the removal of very small particles from a surface, and several laboratory studies of this subject area are reviewed by Zimon [18]. Again, the main difference between these two types of problem is in the particle sizes involved. In the former the particle diameters are often greater than 50 μm and in the latter "cleaning experiments" particles of order 1.0 μm are more common. One important point that does emerge from both sets of observations is that rather large gas velocities must be employed to suddenly dislodge a significant number of particles from solid surfaces.

The steady viscous flow past a small sphere adhering to a solid, plane surface (wall) will not be symmetric, relatively stagnant conditions will exist on the surface near the wall and "suction pressures" will be generated on that portion of the surface of the sphere furthest from the wall. This difference in pressure will result in a "lift" force on the sphere normal to the wall which opposes the adhesive force. Viscous forces in addition will give rise to a drag force. The lift force has largely been ignored by experimentalists [20-23] who have postulated that the particle removal force in fluid flow is approximately equal to the viscous drag. Analyses by Goldman, Cox and Brenner [24] and O'Neill [25] support this assumption. They dealt with the extreme condition of creeping flow, and to this order of approximation, found the lifting force to be negligible compared with the drag force. Air drag forces calculated for particle removal from a theoretical model of the velocity field adjacent to the wall agree within an order of magnitude with forces of removal measured in a centrifuge [20,21,23]. In turbulent flow at removal efficiencies exceeding 25%, that is 25% of particles initially adhering are <u>suddenly</u> removed, air drag calculations and measured gas re-entrainment velocities agree within a factor of 2.5 [23] (see below). From these results, one can infer that particle removal by fluid flow occurs by a

shear mechanism under conditions in which the static coefficient of friction between particle and surface is about unity.

The air drag calculational procedure will be employed here to estimate the mainstream air velocity U_∞ parallel to a surface that is required to dislodge a spherical particle from the surface. We shall consider the steady turbulent flow of air through a parallel plate channel of diameter (gap thickness) D. This flow geometry was employed by Corn and Stein [23] in their study of particle adhesion in an air flow. It is assumed that the air drag acting on a particle adhering to one of the walls of the channel can be calculated as though the particle were alone on the wall and submerged in the laminar sublayer. This simple air drag method should not be regarded as a conservative approach as observed gas velocities causing particle removal sometimes fall below the predicted dislodgement velocities.

Close to the walls the expression for the gas velocity u as a function of distance from the walls y is [26]

$$u = \frac{f\, y\, U_\infty^2}{2\nu} \tag{3.1}$$

where ν is the kinematic viscosity of the flowing gas and f is the friction factor for turbulent flow. The friction factor is evaluated with the Blasius formula applied to the parallel-plate channel:

$$f = \frac{0.0791}{\left(\frac{2\, D\, U_\infty}{\nu}\right)^{1/4}} \tag{3.2}$$

Eliminating f between Eqs. (3.1) and (3.2) yields the velocity distribution near the walls:

$$u = 0.0332\, \frac{y\, \nu}{D^2} \cdot \left(\frac{U_\infty\, D}{\nu}\right)^{7/4} \tag{3.3}$$

Strictly speaking, in a nonuniform velocity field, the drag force must be obtained by integration over the particle projected area. Alternatively, a reasonable approximation can be obtained by calculating the drag force F with the fluid velocity evaluated at the center of the particle (i.e. at y = d/2). The flow around the spherical particle is such that the drag force is well represented by the "intermediate law" [26]:

$$F = \pi \frac{d^2}{4} \cdot \frac{1}{2} \rho u^2 \cdot \frac{18.5}{\left(\frac{du}{\nu}\right)^{0.6}} \tag{3.4}$$

where ρ is the density of the gas. Eliminating the local velocity u between Eqs. (3.3) and (3.4) and setting y = d/2 yields

$$F = 0.0234\, \rho \nu^2 \left[\frac{d^2}{D^2}\left(\frac{U_\infty D}{\nu}\right)^{7/4}\right]^{1.4} \tag{3.5}$$

Finally, assuming that the spherical particle is dislodged when the drag force given by Eq. (3.5) equals the adhesive force given by Eq. (2.4), the particle will leave the surface when

$$U_\infty \geq 9.62 \frac{\nu}{D} \cdot \left(\frac{d}{\rho \nu^2}\right)^{0.4082} \cdot \left(\frac{D}{d}\right)^{8/7} \tag{3.6}$$

In the above expression, all quantities are in cgs units. Note that this result is rather insensitive to the channel diameter D.

We note from Eq. (3.6) that smaller particles appear to adhere more tenaciously in a gas stream, even though the adhesion force between particle and surface is less than that holding larger particles to the surface [see Eq. (2.4)]. The reason for this, of course, is that in an air stream the removal force is dependent on roughly the particle-projected area d^2, while the adhesion force is proportional to d. Letting $\rho = 10^{-3}$ g/cm^3 and $\nu = 0.16$ cm^2/s, corresponding to air at 300°K and atmospheric pressure, we calculate from Eq. (3.6) that a free stream air velocity U_∞ = 184 m/s is required to

remove a 10 μm particle residing on the wall of a 1-cm diameter channel. Thus it would appear that individual particles or even agglomerated particles of overall diameter less than 10 μm are not likely to be removed by hydrodynamic forces in gas flow. In some applications outside of nuclear reactor safety there is an interest in the behavior of a thick layer of particles exposed to a high velocity gas stream. Such particles may be more easily dislodged in large (0.1-10 mm) chunks. The particles adhere tightly to one another, but the large agglomerate they form may extend far outside the laminar boundary sublayer and can be blown (dragged) from the surface. Such thick particle layers, however, are not anticipated to form on the vertical structural surfaces which would be subjected to substantial gaseous flows following containment failure. Thicker layers accumulated on the containment building floor would not be exposed to high velocities. Also, large chunks would fall out of the atmosphere quickly due to their large size.

Given the order of magnitude of the initial radioactive aerosol mass concentration, about 10^{-5} g/cm^3, and the ratio of the containment building volume to the outer wall surface area available for particle deposition in a typical large dry containment, we estimate a uniform deposition layer of only 40 μm in thickness. This thin layer is calculated even after assuming an apparent density of the agglomerated layer lower by a factor of ten from that of the bulk aerosol material density of approximately 4.0 g/cm^3. At air velocities of interest in containment analysis, $U_\infty \sim 10$ m/s, the laminar sublayer thickness is about 160 μm. Thus the aerosol deposition layer is deeply buried in the laminar sublayer and, as demonstrated above, the drag forces are insignificant compared with the adhesion forces. Considering the extensive surface area of internal walls, pipes, structures and equipment as well as the retention of aerosol material within the primary system, this conclusion can be extended to all containment designs.

It is of interest to compare Eq. (3.6) with experimental results on particle removal. Corn and Stein [23] examined particles adhering to a glass or metal substrate before and after exposure to a high velocity parallel-plate channel flow of air. The substrate fitted flush with one of the walls of the channel. Figure 3.1 summarizes the results of such a comparison. We note that at particle removal efficiencies exceeding 90%, re-entrainment velocities

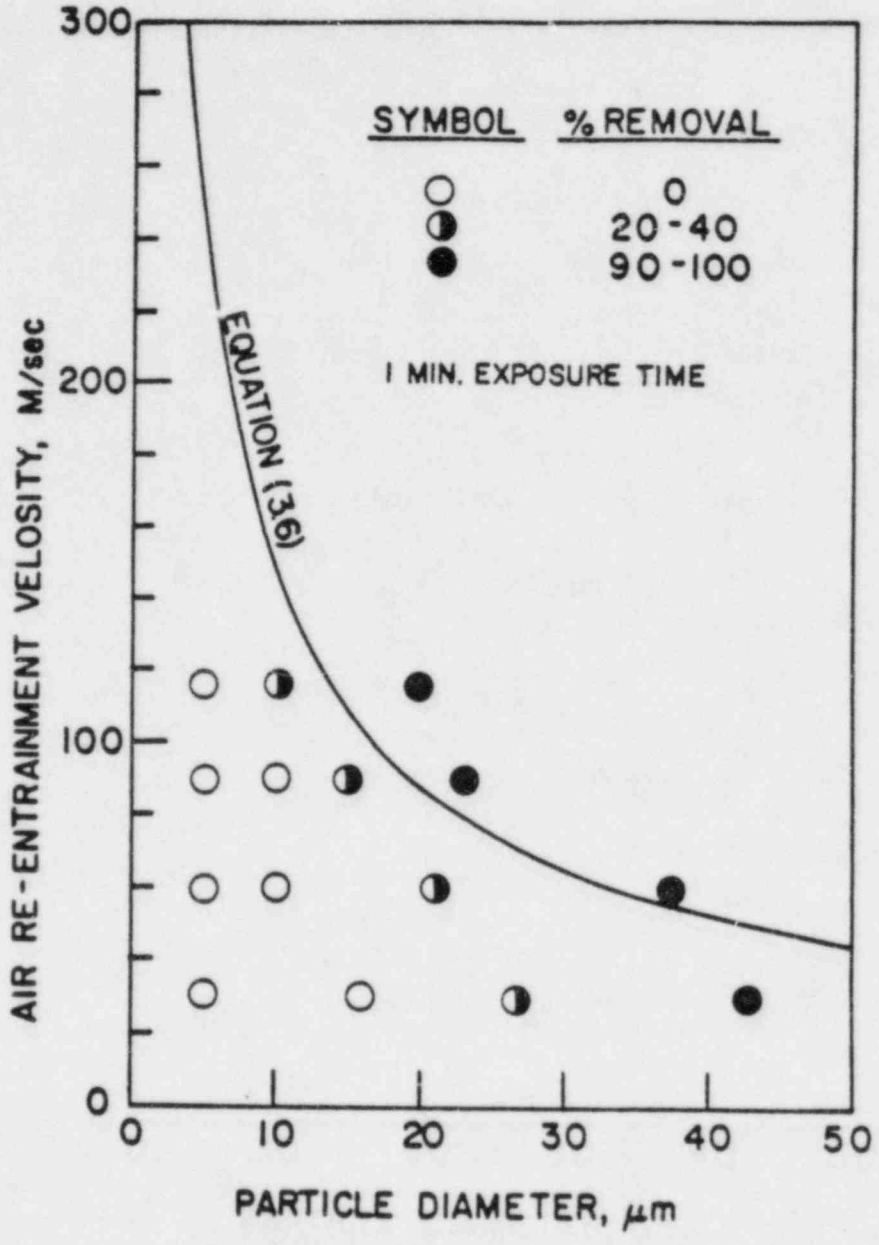

Fig. 3.1 Air re-entrainment of glass beads as a function of particle size; percent removal of beads as a parameter. Comparison of Eq. (3.6) with the data of M. Corn and F. Stein, Ref. [23].

calculated with Eq. (3.6) and measured air velocities are in reasonable agreement. Even at lower removal efficiencies, agreement between theory and experiment is acceptable, with the re-entrainment velocity predictions exceeding by at most a factor of 2.5, the velocities required for incipient entrainment.

The experimental results of Fig. 3.1 are based on a one minute exposure to the channel flow*. As the time of exposure of particles to the air flow is increased, a higher degree of particle removal is observed. Figure 3.2 illustrates the measured time dependency of particle removal by a sustained high velocity air stream. Interestingly enough, this result is in direct contrast with Corn and Steins' [23] companion study of adhesion forces using centrifugation. The time of centrifugation was observed not to influence particle removal efficiencies. Moreover the experimentally determined adhesion forces on the rotor of the centrifuge are in good agreement with the adhesion force equation, viz. Eq. (2.4). Since Eq. (3.6) is based on this empirical adhesion force equation, one can conclude that the air velocity causing a sudden (< 1 min.) high degree of particle dislodgement can be successfully predicted by utilizing air drag theory and experimentally determined adhesion forces. It appears unlikely that one will be able to predict the time dependence of particle removal at lower air velocities. However, for the flow conditions following containment failure, long term removal will not be a significant mechanism since the blowdown characteristics will either be higher velocities and short depressurization time or a long time and very low velocities.

There is other experimental evidence which shows that some particle removal from solid surfaces occurs when the mean flow velocity adjacent to the surface is relatively low. Corn and Silverman [22] carried out experiments on particle removal from a simulated filtration surface (fiber material). Particle removal forces based on air drag calculations and observed resuspension gas velocities were ten times lower than removal forces based on adhesion measured in a companion study. In a similar study, Becker [27] found that

*In terms of containment failure analysis, no significance should be attached to the one-minute exposure time in the experiments of Corn and Stein. We will see later that resuspension throughout the containment is likely to be insignificant regardless of the time of exposure of particles to gas flow.

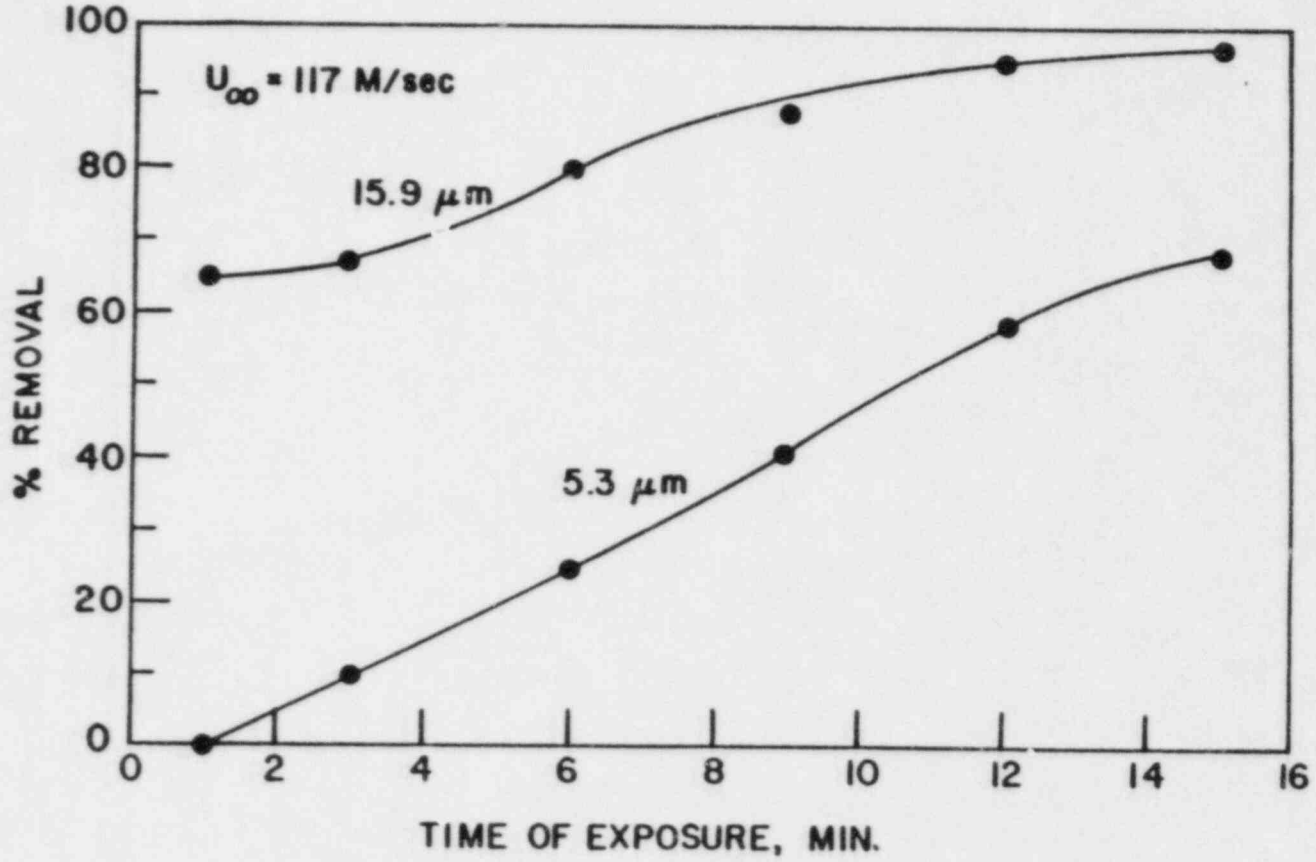

Fig. 3.2 Effect of time of exposure to air flow on particle removal efficiency. M. Corn and F. Stein, Ref. [23].

quartz dusts were removed from filter surfaces at air velocities as low as 0.7 m/s and observed increased particle removal with increased time of exposure to moderate-velocity air streams. Lapple et al. [28] observed the removal of particles at "filtration velocities" from 1 to 3 m/s. As will be discussed, even these velocities are large compared to those anticipated following containment failure.

4.0 MECHANISM OF PARTICLE RESUSPENSION IN TURBULENT FLOW

It is difficult to visualize how some of the small particles in the experiments of Corn and Stein [23] were transported away from the surface at air velocities less than those predicted by boundary layer theory. The deposited particles of glass and fly ash ranged in size from 5 to 40 μm. Such particles are completely engulfed in the laminar sublayer (50 μm thick at U_∞ = 30 m/s) and should be out of range of main stream eddies of turbulence which could possibly dislodge them. Even at gas velocities as high as 117 m/sec, the 5 μm particles are submerged in the laminar sublayer, yet they are dislodged with sufficient time of exposure to the gas stream (see Fig. 3.2). This fact and the observations that increased time of exposure did not increase particle removal in a centrifugal force field led Corn and Stein to the hypothesis that turbulence must penetrate the laminar sublayer.

The idea that the viscous sublayer is not steady and laminar has been discussed by many authors. Direct observations of particles near a solid surface in turbulent flow by Fage and Townsend [29] and by Masoroni and Fish [30] revealed random and unsteady motion attributable to turbulence in the laminar sublayer. Flow visualization studies of the wall region on a flat-plate boundary layer by Kline et al. [31] showed that the sublayer is continually erupting. Corino and Brodkey [32] used 0.6 μm particles to study turbulent motion in the viscous sublayer in pipe flow. Their evidence showed that some particles move away from the wall in sympathy with the turbulent eruptions or bursts. The particles rarely acquire enough momentum to escape from the "laminar sublayer" within the duration of the burst. The ejection of a particle into the main flow seems to occur by means of another turbulent burst. This mechanism involves a competitive process in that some particles which have been detached by one burst are still in the sublayer and could be redeposited before they are carried into the outer turbulent region by a second burst. Cleaver and Yates [33] attempted to predict the rate of removal of particles by combining available formulae for particle lift with literature data on the size and frequency of the turbulent bursts. Unfortunately, the model is not predictive in that it contains an unknown parameter which depends on the type of adhesion force that holds the particles to the surface.

The simultaneous removal of particles by turbulence and redeposition results in a non-zero volumetric concentration of detached particles within the laminar sublayer adjacent to the wall. These detached particles may be thought of as being in "equilibrium" with the particles stuck to the surface, much like gas molecules in equilibrium with an evaporating surface. If the number of detached particles can be specified, a theoretical model can be developed to describe effectively the turbulent resuspension of particles through the boundary layer. The model would be nearly identical to published aerosol deposition (negative resuspension) models and would be based on gas eddy diffusivities and the notion of a particle stopping distance (see e.g. [34,35]). Unfortunately, a way of quantifying the volumetric concentration of detached particles within the sublayer has not yet presented itself and, therefore, estimates of the rate of particle resuspension must rely on experiment.

The experimental work on particle resuspension discussed in the foregoing is of limited use in containment analysis in that the range of air velocities investigated is well above the 0.1-10 m/sec velocity range anticipated following containment failure. Moreover, most of this experimental work was concerned with the measurement of conditions for incipient particle removal rather than the particle removal rate itself. In the next section we review the experimental work which was directed at measuring the rate of particle resuspension.

5.0 THE RESUSPENSION RATE PARAMETER

Almost all of the experimental work on resuspension in turbulent gas flow has been directed toward gaining an understanding of particle movements in the atmosphere near the earth's surface. Much of this work was devoted to the problem of wind erosion of topsoils. Bagnold's [35] pioneering experimental work in the Sahara Desert provided a relationship between wind speed and the total horizontal flux of sand particles. He found the flux of reentrained sand to be proportional to the wind speed cubed. Chepil and Woodruff [36,37] developed a complex wind erosion equation to predict the annual rate of soil loss from a specific agricultural field. Gillette and co-workers [38] have continued experimental research into wind erodibility of various soil textures, confirming many of Bagnold's and Chepil's results.

During the past 20 years, experimental work has been performed to assess resuspension of potentially hazardous materials using inert tracers and, in some cases, radioactive materials. Some of this work can be directly related to the problem of resuspension within a containment building in that solid particles and substrates of different materials were used. The most useful experimental results are those that have been reported in terms of a resuspension rate parameter. By knowing the initial surface mass concentration of solid particles over the substrate surface, χ, the area of the surface sampled, A, the tracer particle mass collected, M, and the duration of the air flow (wind) over this surface, t, a resuspension rate parameter, Λ, can be defined and obtained from experiment via:

$$\Lambda = \frac{M}{\chi A t} \tag{5.1}$$

A more convenient form of this expression for purposes of analysis is

$$\dot{m}_r'' = \Lambda \chi \tag{5.2}$$

where $\dot{m}_r''$ is simply the particle resuspension mass flux [$\dot{m}_r'' = M/(At)$]. The mass concentration of adhering solid particles, χ, is in units of g cm^{-2}, and the resuspension rate parameter Λ has the dimension of $time^{-1}$.

Schmell [39] and Schmell and Lloyd [40] have reported resuspension rate parameters as a function of wind speed. Schmell and Lloyd's data were obtained by seeding a desert soil surface with micron-size calcium molybdate and show Λ proportional to the mean wind speed raised to a power from about one to five, for wind speeds greater than roughly 4 m/s. Their data showed average values of Λ to range between 2×10^{-11} and 8×10^{-8} sec^{-1}.

Perhaps the most well-controlled experimental study of particle resuspension to date is that of Reynolds and Slinn [41]. Particle resuspension was measured in a horizontal flow channel in which known air velocity profiles were generated over a seeded area flush with the channel floor. Zinc sulfide, which is a water insoluble material, was selected as the deposited aerosol particle. The mass mean diameter of the particles was $\sim 3\ \mu m$ (log normally distributed) and a deposition mass of approximately ten grams of particle per square meter of seeded substrate ($\chi \sim 10^{-3}$ g cm^{-2}) was used in all tests. It is interesting to note that the magnitudes of the particle density, and sizes employed by Reynolds and Slinn are similar to those considered in the containment building environment for some accident sequences. The air speed was varied from 2 to 8 m s^{-1} and the time of exposure of the adhering particles to the air speed varied from ten minutes to one hour.

The experimental results of Reynolds and Slinn [41] show average resuspension rates, Λ, to be 1.3×10^{-8}, 2.3×10^{-8}, and 5.6×10^{-8} sec^{-1} for mown grass, fine soil, and gravel substrates, respectively. The measured particle resuspension rate parameter as a function of air speed is shown in Fig. 5.1. A dependence of Λ's on the air velocity, U_∞, of the form $\Lambda \sim U_\infty^3$ was found for the substrates with the least surface moisture content. Lower power dependencies and lower resuspension rates were associated with moist surface conditions. Reynolds and Slinn recommend the following empirical expression for the resuspension rate parameter as a function of air speed for the driest of all gravel substrate samples:

$$\Lambda = 7.39 \times 10^{-10}\ U_\infty^{3.08} \qquad (5.3)$$

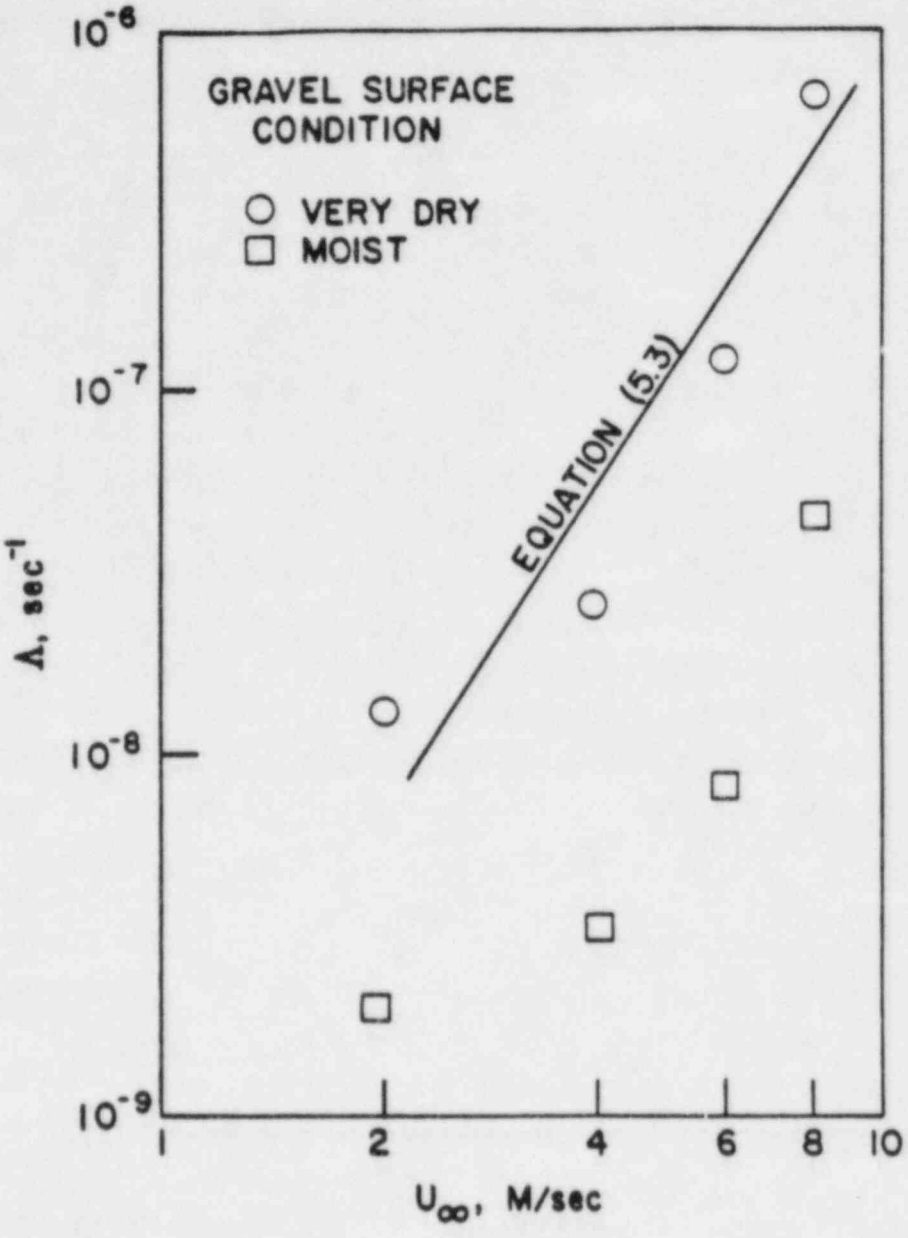

Fig. 5.1 Resuspension rate parameter as a function of air speed. B. W. Reynolds and W. G. N. Slinn, Ref. [41].

where U_∞ is in m/s^{-1} and Λ is in sec^{-1}. Equation (5.3) represents the largest resuspension rates measured by Reynolds and Slinn; it is in good agreement with resuspension rate measurements of zinc sulfide particles from an asphalt surface [39].

It should be mentioned that to this writer's knowledge no measurements have been made of the resuspension of particles in a vertical air flow. Gravitational settling (or redeposition) can have an important effect in horizontal flows. Consequently, the resuspension rate given by Eq. (5.3) may be less than that for vertical flows under otherwise identical conditions. However, correlations obtained from experiments with horizontal flows can be used to estimate resuspension (or deposition) rates for vertical flows if the gravitational settling velocity is small compared with the turbulent transport velocity within the boundary layer. It can be shown that, for particles with diameters from 3.0 to 10.0 μm and density of approximately 4.0 g cm^{-3}, Eq. (5.3) is applicable for high-velocity vertical flows with $U_\infty \gtrsim 10.0$ m s^{-1}. Since containment gas velocities as high as 10.0 m s^{-1} are of interest in the analysis of postulated degraded core accidents, Eq. (5.3) will be exploited in a subsequent section to determine the potential for entraining deposited, radioactive aerosol particles off of both horizontal and vertical surfaces within the containment building.

Before leaving this section, a word of caution should be inserted here. Equation (5.3), though valuable for aerosol transport analysis, should not be considered valid for all substrate materials. This empirical relation is based on resuspension from rough natural surfaces and should be accurate for surfaces of similar roughness, such as concrete. A high percentage of the aerosol particles within the containment, however, will deposit on steel surfaces. It has been observed [41,42] that resuspension rates increase as the roughness of the surface decreases (see Fig. 5.2). In fact, the few measurements made by Sehmel [42] on resuspension rates of dry 10 μm uranine particles from a smooth aluminum surface indicate Λ's that are three orders of magnitude higher than those for gravel and asphalt*. Nevertheless, as will be

*It is not clear as to why this is the case. One can only speculate that very rough surfaces having projections (cracks, chips, etc.) with heights much greater than the thickness of the particle deposit shield the particles from the cross flow of air and thereby tend to retain the particles.

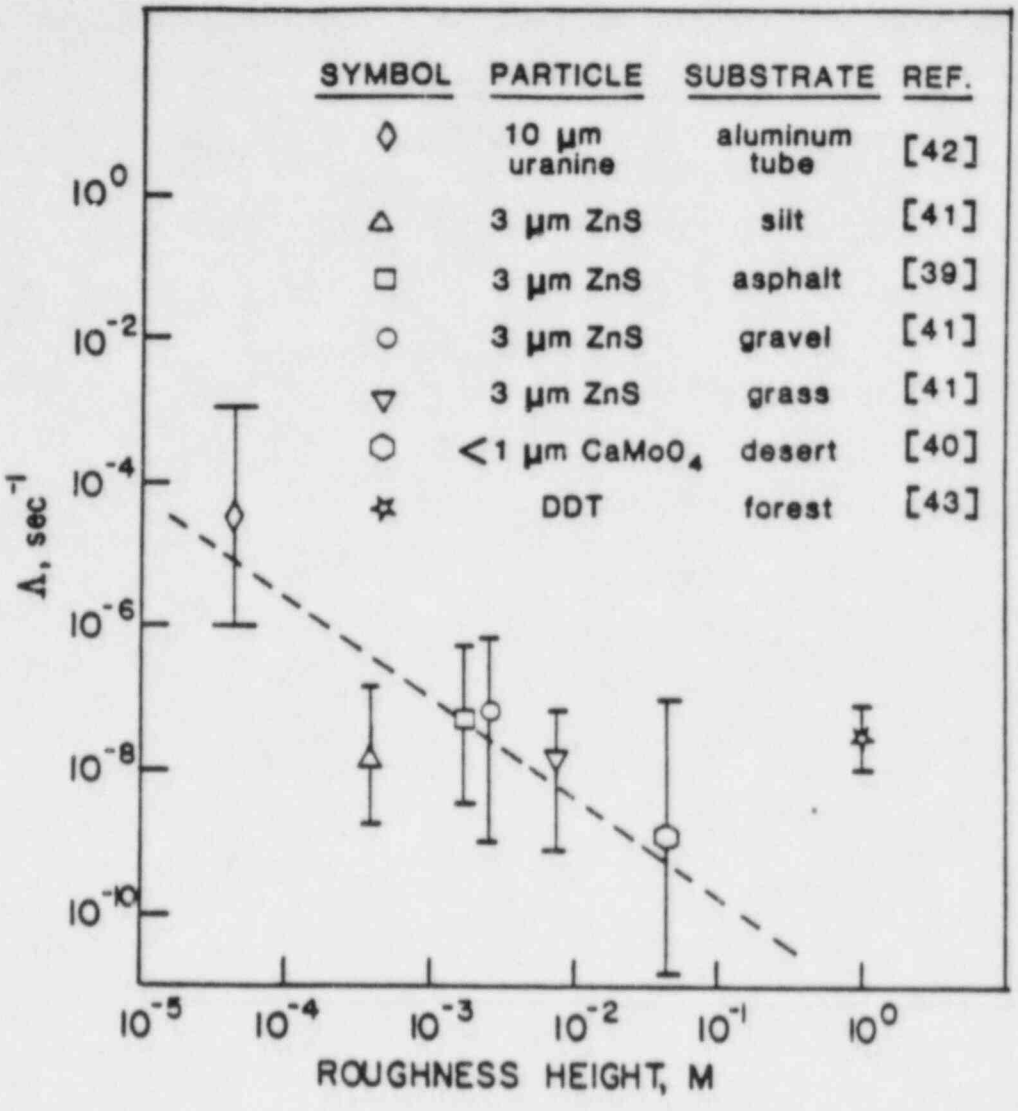

Fig. 5.2 Average resuspension rate parameter from various surfaces as a function of surface roughness height. The dashed line represents a least squares fit of the data (excluding the DDT data) proposed by Reynolds and Slinn [41]. The symbols □, △, etc. represent the average resuspension rate of the range of values obtained in each case.

demonstrated in a later section, Λ's much higher than those measured for smooth surfaces are required to create significant resuspension following containment failure.

6.0 CONTAINMENT BLOWDOWN

The specific physical geometry for which the time scale of the blowdown is calculated is dependent upon the specific failure mode of the containment building. Several different failure modes can be considered such as a failure location at the top or dome of the structure and a failure site lower in the containment around penetrations. Models are developed for both failure sites and are applied to the specific containment designs in IDCOR Task 23.1 [44-47]. Failure near the top of the containment will be considered first with penetration type failures considered secondly.

6.1 Failures in the Upper Region of the Containment

The containment building atmosphere is assumed to flow in a one-dimensional manner in the upward z-direction to the elevated failure location. Because the containment gas cannot pass through the floors of the building compartments, the gas velocity must be zero at this boundary and within a compartment. Consequently, the maximum velocity will be at the top of the failed compartment. For the analyses of large rupture sites, the velocities addressed will be the one-dimensional values near the failure site. This is a conservatism in the modeling approach increase with increasing elevation. Since the pressure drop from the floor of the containment to the dome is very small compared to that at the failure location, the containment gas density ρ is independent of height z. Thus, by integrating the one-dimensional, gas continuity equation we find that the main stream velocity U_∞ is directly proportional to z according to*

$$U_\infty = - \frac{d \ln \rho}{dt} \cdot z \qquad (6.1)$$

The maximum mass flow rate which can pass through the failure hole is given by the well-known single phase compressible flow result for maximum or "choked" flow

*Equation (6.1) also represents the local vertical velocity within adherent layers of particles on the horizontal surfaces within the containment building. The potential for this velocity to disrupt settled particle layers will be demonstrated by experiments and analyzed later in this report.

$$\dot{m} = A_H \cdot \left[\gamma P_\rho \left(\frac{2}{\gamma + 1} \right)^{\frac{\gamma+1}{\gamma-1}} \right]^{1/2} \tag{6.2}$$

where $\dot{m}$ is the mass flow rate in grams per second, A_H is the area of the hole, P is the instantaneous containment pressure and γ is the ratio of specific heats. The mass balance for the entire containment building is

$$V \frac{d\rho}{dt} = - \dot{m} \tag{6.3}$$

where V is the volume of the building. Combination of Eqs. (6.2) and (6.3) then gives

$$\frac{d\rho}{dt} = - \frac{A_H}{V} \left[\gamma P_\rho \left(\frac{2}{\gamma + 1} \right)^{\frac{\gamma+1}{\gamma-1}} \right]^{1/2} \tag{6.4}$$

When the containment blowdown process is of reasonably short duration, as in the case of large failure holes, the containment depressurization is approximately adiabatic. Therefore, for an ideal containment gas,

$$\frac{P}{P_o} = \left(\frac{\rho}{\rho_o} \right)^{\gamma} \tag{6.5}$$

where the subscript o refers to containment atmosphere conditions at the instant of failure. We may now use Eq. (6.5) to eliminate P from Eq. (6.4) and by integration obtain an expression for the elapsed blowdown time as a function of the density of the gas remaining in the containment:

$$t = \frac{V}{A_H} \left[\gamma R T_o \left(\frac{2}{\gamma + 1} \right)^{\frac{\gamma+1}{\gamma-1}} \right]^{-1/2} \cdot \left(\frac{2}{\gamma - 1} \right) \cdot \left[\left(\frac{\rho_o}{\rho} \right)^{\frac{\gamma-1}{2}} - 1 \right] \tag{6.6}$$

where R is the ideal gas constant and T_o is the temperature of the containment gas at the instant of failure.

For the case of small failure holes, there is sufficient heat transfer from structure to gas within the containment to make the depressurization approximately isothermal. In this limiting case Eq. (6.5) with $\gamma = 1$ is substituted in Eq. (6.4) and the result is integrated to obtain

$$t = \frac{V}{A_H}\left[\gamma RT_o\left(\frac{2}{\gamma+1}\right)^{\frac{\gamma+1}{\gamma-1}}\right]^{-1/2} \cdot \ln\frac{\rho_o}{\rho} \qquad (6.7)$$

As we shall see below, for density ratios ρ_o/ρ of practical interest, say $\rho_o/\rho < 10$, both the adiabatic and isothermal limiting cases result in almost identical predicted blowdown times.

Let us assume that a rather large containment failure hole of area $A_H = 10\ m^2$ forms when the containment atmosphere's temperature and pressure reach $T_o = 600°K$ and $P_o = 10.0$ atm. This is the largest failure area identified in the Task 23.1 report for Zion [44]. A containment design of volume $V = 5 \times 10^4\ m^3$ and height $z = 60$ m is assumed and the containment gas is assigned the properties of air ($\gamma = 1.4$; $R = 2.87 \times 10^6\ cm^2\ s^{-2}\ °K^{-1}$). The magnitude of the containment discharge time through the failure location can be calculated from Eq. (6.6) or (6.7). Strictly speaking, these relations are not valid after the ratio of the containment pressure to the ambient pressure, P/Pa, falls below the critical pressure ratio

$$\frac{Pa}{P} = \left(\frac{2}{\gamma+1}\right)^{\frac{\gamma}{\gamma-1}} \qquad (6.8)$$

A reduction in P below this critical value results in a subsonic mass discharge rate that is dependent on the ambient density (or pressure). For high initial containment pressures P_o relative to ambient, the duration of the "subsonic discharge period" is short compared with the "choked-flow discharge period" and it can be neglected. From Eq. (6.6) we estimate that it takes only 22 seconds for the containment air density to be reduced to the critical

value given by Eq. (6.8)*. The corresponding isothermal discharge time is 19 seconds. At this point in time the containment air density is about 68 percent less than its initial density (ρ/ρ_o = 0.325), the containment pressure is about 80 percent less than its initial pressure (P/P_o = 0.207), whereas from Eqs. (6.1) and (6.4) we find that the local gas velocity U_∞ is only reduced by 20 percent for adiabatic containment depressurization and zero percent for isothermal depressurization during the time choked flow prevails at the failure location. Note from Eq. (6.4) that $d\ln\rho/dt \sim T^{1/2}$, so that for isothermal flow U_∞ is time invariant. Thus during blowdown, U_∞ remains fairly constant in time while the flow through the failure location is choked and then rapidly drops to zero during the subsequent period of subsonic flow at the failure location, which for our sample problem has been calculated to last for only about 4 seconds.

6.2 Local Failures Around Penetrations

As containment pressurization increases to the state of general yield, the areas of highest strain, such as the regions around the penetrations, could experience local tears in the liner or the penetration itself. These would continue to grow until the failure area equals that required to terminate the penetration. Flow through this hole would be choked as were the cases considered in Section 6.1. Figure 6.1 illustrates the mass flow ($\dot{m}$) through the failure site as given by

$$\dot{m} = \rho_t A_H U_t \tag{6.9}$$

where ρ_t is the gas density at the choking (sonic) location, U_t is the sonic velocity and A_H is the failure area. For this representation it is sufficient to assume the sonic velocity is 500 m/sec and also that the gas density within the containment (ρ_o) is twice that at the choking location. If the flow acceleration to the failure site is assumed to occur hemispherically, continuity dictates

*It should be noted that these evaluations ignore the pressurization source which is negligible for large break sizes but would be important if the rupture area is of the order 0.01 m^2.

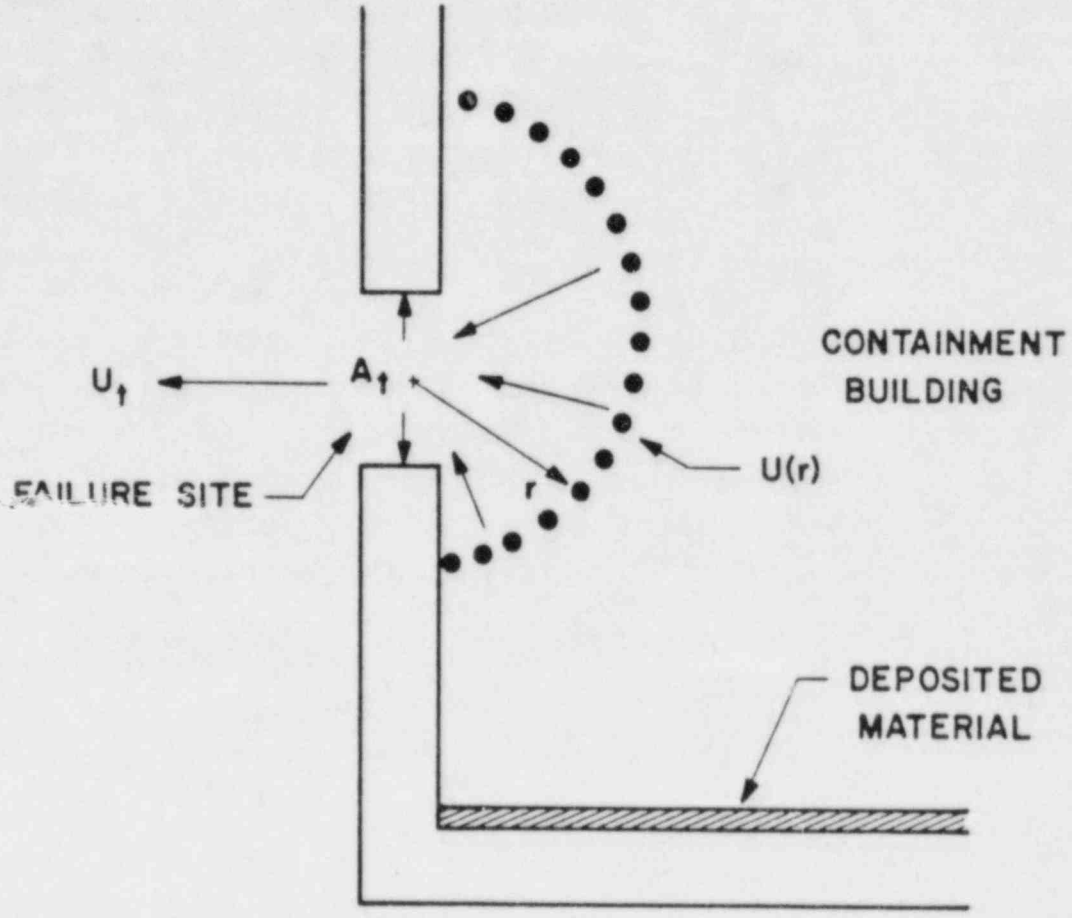

Fig. 6.1 Radial flow toward a localized failure site.

$$\rho_t A_H U_t = \frac{\rho_o}{2} \pi r_H^2 U_t = \frac{\rho_o}{2} 2\pi r^2 U(r) \qquad (6.10)$$

where r_H is the effective radius of the failure. The gas velocity in the immediate vicinity of the failure as a function of the radius from the rupture (r) is given by

$$U(r) = \frac{1}{2}\left(\frac{r_H}{r}\right)^2 U_t \qquad (6.11)$$

A rupture size of about 0.05 effective radius or less is sufficient to prevent pressurization. Therefore, the velocities at a radius of 1 m are reduced to 1.25 m/sec, which is one or two orders of magnitude below those required for a significant entrainment rate of deposited material. For a distance 2 m from the rupture, which is more typical of the penetration elevation above the containment floor, the velocity is reduced to about 30 cm/sec. The entrainment rate given by Eq. (5.3) is approximately 2×10^{-10} sec^{-1} which results in negligible resuspension.

7.0 PARTICLE RESUSPENSION FOLLOWING REACTOR VESSEL OR CONTAINMENT FAILURE

7.1 Containment Failure

7.1.1 Failure in the Upper Region of the Containment

The one-dimensional model for flow to a rupture high in the building is used along with an assumption of a uniform volumetric particle concentration at any z plane except within the thin turbulent boundary layers adjacent to the structural surface, which are contaminated with deposited aerosol particles. The local surface area per unit volume of containment building atmosphere is assumed constant, that is independent of z, and therefore equal to the total surface area S divided by the total containment volume V.

At any location z, re-entrained aerosol particles are introduced into the upward flowing containment atmosphere at the mass flux given by Eq. (5.2). Some of the aerosol particles carried by the gas flow will re-deposit on the bounding surfaces in accord with the usual particle mass-transfer relation [33,34]:

$$\dot{m}''_d = Kc \tag{7.1}$$

where $\dot{m}''_d$ is the mass rate of deposition per unit area of surface and K is the mass-transfer coefficient in units of velocity. In order to calculate K we have chosen the correlation recommended by Friedlander and Johnstone [33], Liu and Agarwal [49], and McCoy and Hanratty [50]:

$$\frac{K}{U_\infty} = 3.25 \times 10^{-4} \left(\frac{f}{2}\right)^{1/2} \left[\left(\frac{f}{2}\right) \frac{d^2 \rho_p U_\infty^2}{18 \nu^2 \rho}\right]^2 \tag{7.2}$$

where f is the friction factor for turbulent flow over a flat plate and ρ_p is the density of the particle material. (This expression ignores deposition due to sedimentation, which could dominate for horizontal surfaces.) Equation (7.2) is the best average fit of the available data for particle diameters, d,

and free stream velocities, U_∞, such that the dimensionless group in brackets lies within the range 0.2-22.5.

Performing a differential particle mass balance over an element of containment height ∂z, we find that the particle mass concentration within the containment gas satisfies the partial differential equation

$$\frac{\partial c}{\partial t} + \frac{\partial c\, U_\infty(z)}{\partial z} = \frac{S}{V}\left[\Lambda(z) \cdot \chi - K(z) \cdot c\right] \tag{7.3}$$

The mass balance equation for the particle's concentration on the surface, χ, is

$$\frac{\partial \chi}{\partial t} = k(z) \cdot c - \Lambda(z) \cdot \chi \tag{7.4}$$

Note that both K and Λ are power law functions of height z, since $K \sim U_\infty^5$, $\Lambda \sim U_\infty^3$ and $U_\infty \sim z$ from Eqs. (7.2), (5.3) and (6.1). Equations (7.3) and (7.4) are linear in c and χ and can, in principle, be solved by linear techniques, such as the method of LaPlace transforms. However, it is not intended here to present a detailed mathematical treatment of these equations, but, instead, to to assess the significance of particle resuspension following containment failure.

For this assumed failure site with the most rapid depressurization, the maximum one-dimensional gas velocity within the containment atmosphere occurs at the top of the building near the failure location (but far enough below the failure hole so that the gas velocity is one-dimensional). This is far removed from horizontal surfaces where comparatively thick layers could accumulate. Let us make the conservative assumption that <u>all</u> the surfaces (except the containment floor which would not experience tangential flows) within the containment building are submerged in a free stream flow with a tangential velocity equal to the maximum value. In addition, it is conservatively assumed that all surfaces are uniformly covered by particle layers of the same surface concentration χ. Clearly, both of these assumptions will result in overestimates of the particle resuspension rate. The height

variations of U_∞, Λ and K are now ignorable and the z-independent solution of Eqs. (7.3) and (7.4) is readily determined to be

$$c = \frac{(\chi_o\ S/V + c_o)\Lambda - (\Lambda\ \chi_o\ S/V - K\ c_o\ S/V) \cdot e^{-(\Lambda + K\ S/V)t}}{\Lambda + K\ S/V} \qquad (7.5)$$

where c_o and χ_o are the volumetric and surface particle concentrations at the instant of containment failure.

To further simplify matters, let us suppose that all of the aerosol material released to the containment building is deposited during the time period following reactor vessel failure but before containment failure. Thus we have the initial condition $c_o = 0$ at $t = 0$ for the blowdown event, and Eq. (7.5) reduces to the simple form

$$\frac{c}{c_R} = \frac{\Lambda\left[1 - e^{-(\Lambda + K\ S/V)t}\right]}{\Lambda + K\ S/V} \qquad (7.6)$$

where c_R is the release concentration of the aerosol, or the total mass of the aerosol material divided by the volume of the containment ($c_R = \chi_o\ S/V$). The ratio of the particle concentration in the gas to the release concentration, c/c_R, is a measure of the potential for resuspension.

Returning to the sample problem in Section 6.1, we predict a maximum gas velocity $U_\infty = 1.7$ m s^{-1} by setting $z = 60$ m in Eq. (6.1). Assuming a particle mean diameter $d = 3\ \mu m$ and particle density $\rho_p = 4.0$ g cm^{-3}, we calculate from Eq. (7.2) a deposition mass transfer coefficient $K = 2.4 \times 10^{-6}$ cm s^{-1}. Equation (5.3) for the resuspension rate parameter leads to the estimate $\Lambda = 4.3 \times 10^{-9}\ s^{-1}$. The surface area S within the containment building is about $10^5\ m^2$ so that the ratio $S/V = 10^{-2}\ cm^{-1}$. From these estimates we infer from Eq. (7.6) that the mass fraction of the aerosol concentration released to the containment building and resuspended as a result of containment failure and the subsequent 22-sec blowdown process is only $c/c_R = 10^{-7}$. As pointed out earlier, Eq. (5.3) is based on resuspension measurements from rough, natural surfaces and that the value of Λ may have to be

increased by roughly three orders of magnitude to $\Lambda = 10^{-4}$ s^{-1} in order to better represent resuspension from the metal surfaces within the containment building. In this case the mass fraction of aerosol resuspended would increase to $c/c_R \approx 10^{-4}$. Clearly, the amounts of radioactive aerosol material resuspended from either rough surfaces or metal surfaces during the relative short time frame of a containment failure and depressurization event is very small even for large rupture sizes.

This conclusion is for a specific example involving a large containment failure hole. The question naturally arises as to whether resuspension could be significant with small containment failure holes, since the blowdown time, t, increases with decreasing failure hole area A_H. The airborne particle concentration c is proportional to Λt and t is proportional to $1/A_H$. However, the resuspension rate parameter, Λ, is proportional to the local containment gas flow raised to a power. For dry surface conditions $\Lambda \sim U_\infty^3$ and, since $U_\infty \sim A_H$, $\Lambda \sim A_H^3$. It follows that the particle gas concentration is linked to the size of the failure by $c \sim A_H^2$. Thus a decrease in the size of the failure hole acts to lessen the resuspension potential.

It is interesting to examine the limiting case of Eq. (7.6) of an infinitely long containment blowdown. In this extreme $t \to \infty$ and Eq. (7.6) becomes

$$\frac{c}{c_R} \to \frac{\Lambda}{\Lambda + K\, S/V} \tag{7.7}$$

corresponding to a balance between deposition and resuspension. This equation reveals that, because of the redeposition process, the containment gas particle concentration can never return to its initial release value, c_R, by resuspension. Using our previous estimates $\Lambda = 4.3 \times 10^{-9}$ s^{-1}, $K = 2.4 \times 10^{-6}$ cm s^{-1}, and $S/V = 10^{-2}$ cm^{-1}, we get $c/c_R \to 7.1 \times 10^{-3}$ as $t \to \infty$, suggesting that substantial resuspension will never occur in the example case selected.

7.1.2 Local Failures Around Penetrations

As discussed in Section 6.2, stretching of the containment due to long term overpressure could result in local failures at penetrations that are located 2 to 3 m above the containment floor. Such failures could also result if the failure were due to an overtemperature condition. These ruptures would only open a sufficient amount to terminate the pressurization, but the flow could exist for over a long interval.

Equation (6.11) shows the velocity toward the rupture decreases as distance squared. Assuming penetrations to be 2 m above the containment floor, the tangential velocity across the top of the debris layer settled on the floor in the near vicinity of the rupture would be about 0.16 m/sec. For this velocity, the mass transfer coefficient K is 4.3×10^{-10} cm/sec and the resuspension rate parameter Λ is 2.6×10^{-12} sec^{-1}. Using Eq. (3.5), the entrainment rate can be expressed as a function of the distance to the rupture site. Since the resuspension parameter varies as the velocity cube, it will depend upon this distance to the sixth power. The actual mass resuspended can be calculated by integrating over the entire floor area. In the absence of complete integration, we can conservatively assume the value calculated above applies to the entire floor area. If it is also assumed that the inert aerosols are ten times greater than the cesium iodide, and cesium hydroxide, which are approximately 200 kg. Therefore, the inert aerosols would be 2000 kg, which would result in an aerosol loading density of about 2 kg/m^2. (A floor area of 1000 m^2 was assumed.) Resuspension of this mass would require approximately 10 years, which from a practical standpoint means no significant resuspension would occur at containment failure. It should also be remembered that this simplified analysis greatly overestimates the resuspension rate since the strong variation within distance from the rupture was ignored.

In conclusion, the analyses for entrainment as a result of tangential flows, both for localized penetration failures low in the containment and larger failures in the upper regions, show that deposited aerosol material would not be resuspended at the time of containment failure. This leaves disruption of debris beds due to depressurization as the only potential means

of resuspension. Experiments addressing this mechanism are discussed in the next section.

7.2 Reactor Vessel Failure

While the experimental data base is more closely related to accident conditions within containments in terms of pressures and temperatures, the basic models described in the previous sections can be extrapolated to primary system conditions to estimate the resuspension potential immediately following reactor vessel failure. For accident sequences in which the primary system is at an elevated pressure prior to RPV failure, the subsequent blowdown could potentially resuspension previously deposited aerosol material in various regions of the primary system. The major difference in this assessment and that for the containment is the pressure at the time of RPV failure, which principally influences the gas density. Primary system pressure and system geometry will be discussed for the specific conditions of interest in PWR and BWR geometries.

7.2.1 PWR Specific Considerations

IDCOR PWR reference plants include Zion, a Westinghouse NSSS with a large dry containment, and Sequoyah, a Westinghouse NSSS with an ice condenser containment design. The dominant accident sequences include station blackout for both systems and a small break loss-of-coolant accident (LOCA) for Sequoyah. In these accident scenarios, the primary system will be at an elevated pressure when the vessel fails. With the localized failure at in-core penetration [51] the vessel breach diameter created by the corium discharge would be about 0.3 m, or an area (A_H) of approximately 0.07 m^2. Assuming the gaseous blowdown to progress in an isothermal manner, the primary system pressure (P_o) is expressed by

$$\frac{dP_o}{P_o} = \frac{n\, A_H}{V} \sqrt{RT}\, dt \qquad (7.8)$$

where η is the isothermal critical pressure ratio (0.6), V is the primary system volume, R is the gas constant (assume steam) and T is the absolute temperature for the primary system. This can be integrated to give

$$\frac{P}{P_o} = e^{-\frac{\eta A_H \sqrt{RT}}{V} t} \tag{7.9}$$

where P_o is the primary system pressure at the initiation of blowdown. For a primary system volume of 300 m^3, the pressure would decay to 5% of the initial value, or 0.78 MPa, in 40 secs and to 0.19 MPa within 60 secs. Thus, the blowdown would only last about one minute.

The flow area (A_F) through the hot leg and cold leg piping is about 5 m^2. Continuity dictates that

$$\rho_o A_F U = \eta \rho_o A_H \sqrt{RT} \tag{7.10}$$

where U is the gas velocity in the coolant legs. Thus, the velocity through these lines would be about 4.4 m/sec. This is particularly important for the PWR since the horizontal section of the hot legs could have fission products deposited before vessel failure. For example, in Ref. [44], 80 kg of inert aerosols, 40 kg of cesium iodide and cesium hydroxide, and 7 kg of tellurium are calculated to be deposited in the hot legs for a station blackout prior to vessel failure. The resuspension potential must be evaluated for these high pressure, high density conditions.

Equation (3.6) characterized the potential for overcoming the adhesive forces for dry particles. This shows the velocity required for removing particles various approximately as the inverse of the square root of the gas density. Therefore, at pressures of 15.5 MPa, the entrainment velocity would be reduced about 12 times from that required at 0.1 MPa. Considering particle sizes of 10 μm and less, which are those calculated to be deposited in the hot legs, reentrainment velocities would be about 10 m/sec, i.e. well in excess of those available. Also, as the pressure decreases in the blowdown, the required velocity would increase whereas the actual velocity would

remain approximately the same. Thus, the potential for complete entrainment would be insufficient at the start of blowdown and would continually decrease thereafter.

The rate of entrainment can be considered by extrapolating Eq. (5.3), which is derived from experimental data at one atmosphere, to reactor system conditions. Assuming the gas dynamic pressure (ρU^2) controls the rate of resuspension over long time intervals, the resuspension rate parameter, which varies as the velocity cubed, can be extrapolated based upon a density to the three halfs power*. This would give

$$\Lambda = 1.4 \times 10^{-6} U_{\infty}^{3.08} \tag{7.11}$$

at 15.5 MPa, or a value of $\Lambda = 1.9 \times 10^{5}$. With a settling area of about 20 m^2 and a settled mass concentration of 6.4 kg/m^2, the long term resuspension rate would be 2.4×10^{-3} kg/sec or less than 150 g of aerosol during the entire blowdown (60 secs). (This overstates the resuspension since the potential for resuspension decreases as the pressure decreases.) Therefore, there is little potential for resuspension in the hot legs of the reactor coolant system (RCS).

Conditions within the upper plenum must also be considered. However, this is somewhat different in that the temperature would be sufficiently high that the cesium iodide and cesium hydroxide would be liquid, likely quite thin (less than 1 mm) due to the limited mass, and very adherent. The cesium hydroxide, which could dissolve the cesium iodide could chemically attack the stainless steel structures cause the materials to stick to the surface. Also, the flow area is about 10 m^2 which would reduce the gas velocity to about 1.5 m/sec or less. The velocity required to directly entrain liquid films at this pressure would be about 2.5 m/sec and would increase as the pressure de-

*"Entrainment forces" are usually proportional to the product of the gas velocity and the square-root of the gas density. Considering the nearly cubic relationship between Λ and U_{∞}, it seems appropriate to extrapolate according to a three-halves power law.

creases*. Therefore, with the combination of a tightly adhering liquid state, possible chemical reactions with the surface, insufficient gas velocities for direct entrainment, thin liquid films and the potential for being held up on various horizontal structures, the potential for resuspension due to tangential flows in the upper plenum of PWR systems would also be small.

In summary extrapolation of the available data base to PWR system conditions at the time of RPV failure leads to the conclusion that previously deposited aerosols would not undergo significant resuspension during the blowdown. This is the case for both station blackout and the small break LOCA; the only fundamental difference being the primary system pressure at the RPV failure.

7.2.2 BWR Specific Considerations

IDCOR BWR reference plants include Peach Bottom, a General Electric NSSS with a Mark I containment, and Grand Gulf, a General Electric NSSS with a Mark III containment. The dominant accident sequences include a loss of suppression pool cooling, an anticipated transient without scram (ATWS), station blackout and LOCAs. In general the BWR system is easier to evaluate for primary system resuspension than the PWR.

First, most of the sequences identified for the BWR involve actuation of the automatic depressurization system (ADS). Consequently, the primary system is depressurized at the time of reactor vessel failure and there is no potential for resuspension.

---

*This velocity can be estimated through the expression

$$U = \frac{K \sqrt[4]{g\sigma(\rho_\ell - \rho_g)}}{\sqrt{\rho_g}}$$

where g is the acceleration of gravity, σ is the liquid-vapor surface tension and ρ_ℓ and ρ_g are the densities of the liquid and gas phases respectively. The parameter K is the Kutateladze number and has been experimentally determined to be 3.7 for direct entrainment of liquid films.

Secondly, the upper plenum configuration contains separators and dryers designed to remove small liquid particles from the gas stream. Those which are removed would be collected on the bottom of the separators and driers and if they are liquid or are lubricated by liquid drain into the shroud region where water generally remains. In either location they would not be exposed to tangential flows during vessel blowdown. Those particles which are not removed by the separators and driers would be discharged to the suppression pool and would be permanently retained.

Thirdly, the shroud region contains large quantities of water below the jet jump throats which can capture and retain the aerosol particles. Also, the flow from the shroud region is limited by the jet pump throat area. These velocities are limited and would not provide significant resuspension.

Fourthly, there are no horizontal areas which experience large tangential flow velocities. Also, the only significant horizontal area for deposition is the base of the separators where there is only a small tangential flow component.

Lastly, for accident sequence definitions where the primary system is not depressurized at the time of vessel failure, the analysis derived for the PWR is also applicable to the BWR. However, the initial pressure is 7 MPa or less, which reduces the potential for resuspension which was already concluded to be insignificant for the PWR systems.

In summary extensions of the available data base for resuspension to the primary system conditions during gaseous blowdown after RPV failure shows this potential to be small. Consequently, it is recommended that the integrated analyses consider aerosol deposited within the primary system prior to vessel failure to remain deposited during the primary system blowdown.

8.0 DISPERSION OF SETTLED AEROSOL PARTICLES

8.1 Introduction

Accident analyses (Refs. [44] through [47]) show that sedimentation is a major mechanism for removing aerosols from the primary system and containment atmospheres during various stages of the accident sequence. Before considering the behavior of dry beds of fine particles, the physical state of influential aerosols should be considered. The following sections first discuss simple experiments on the physical state of cesium iodide and cesium hydroxide as influenced by moisture in the containment building and secondly present experiments and analyses on the dispersion of settled particles by depressurization.

8.2 Physical State of Cesium Iodide and Cesium Hydroxide

IDCOR Task 11.1 [52] evaluated the dominant chemical species for various fission products. For cesium and iodine, which have a major influence on the public health risk, the dominant species for iodine was cesium iodide with the remaining cesium in the form of cesium hydroxide. Since both of these are highly soluble in water and since many accident sequences have considerable water in the containment at the time these materials are released from the fuel, the physical state in the presence of limited water must be determined.

For pressure suppression containment designs with large quantities of ice or water, cesium iodide and cesium hydroxide dissolved in the water would remain there and would not be subject to dispersion forces. The material of principal interest here is that which may have been exposed to limited quantities of water (steam in the atmosphere or water on the containment floor) which subsequently evaporates due to decay heat.

In separate experiments, a few grams of stable cesium iodide and cesium hydroxide were dissolved in 50 ml of water to simulate deposition on a water covered surface. A sample of each solution was put on a glass slide and exposed to a heat lamp under atmospheric conditions for sufficient time to

either dry the solution or develop a steady state condition. The cesium iodide solution dried out leaving the previously dissolved material as a tightly adhered white deposit on the glass surface that could only be removed by scrapping. In contrast, the cesium hydroxide solution never dried out. In steady state, it became a thick, pasty substance which was tightly adhered to the glass surface. Thus, a small amount of moisture in the atmosphere will ensure that cesium hydroxide will remain wet.

These results demonstrate that the history of fission products in the containment can have a significant influence on their physical state at the time of containment failure. In particulate, it determines whether deposited aerosols remain as individual particles or develop into a more coherent deposit.

8.3 Resuspension Potential of Dry Deposits

These experiments provide a demonstration of the depressurization rates required to levitate well defined particulate and can be compared with the fundamental model for fluidization of a particulate layer. This model can then be extrapolated to depressurization rates considered for hypothetical core damage accident scenarios for specific reactor systems.

Dispersal due to fluidization is treated by Fuchs [53] and it is reported that fine particle sizes can be fluidized by a gas stream. For these evaluations, the fluidization velocity results from the depressurization of the primary system or containment. Thus, the basic conditions in the experiments should address meaningful velocities. In particular, these experiments investigate a range of depressurization rates which bound those considered for the primary system and containment. The influence of such depressurization histories on spherical glass particulate is quantified for particulate sizes of approximately 10 microns particle diameter. Specifically, the depressurization rate required for significant mass loss from the particulate layer is determined and compared with the prediction of a basic particulate levitation model.

8.3.1 Basic Considerations for Particulate Levitation

As in Section 6, consider the containment to be a large volume with a hole at the top, the depressurization can be simply approximated by assuming that the blowdown process is isothermal. With the constant volume condition for the containment, the depressurization rate can be specified by [see Eq. (6.3)]

$$\frac{dP}{dt} = - \frac{RT}{V} \dot{m} \tag{8.1}$$

where R_m is the gas constant for the mixture in the containment (assumed to be a value of 300), T_g is the temperature of the gaseous media, V is the containment volume and $\dot{m}_g$ is the mass flow rate through the break. The mass discharge through the break rate can be represented as an isothermal choking condition

$$\dot{m}_g = \rho A_H \sqrt{RT} \tag{8.2}$$

and substituting this into the expression for the depressurization rate, an expression for the initial rate is given by

$$\frac{dP}{dt} = \frac{n A_H \sqrt{RT}}{V} P_o \tag{8.3}$$

where P_o is the containment pressure at failure and n is the isothermal critical pressure ratio (0.6). Assuming a break area of 10 m^2, (the largest credible size determined by the containment rupture analysis in Ref. [47]) a gas temperature of 500°K and the containment volume of 70,000 m^3, the initial depressurization rate would be 3.3×10^4 Pa/s. Since this would be the initial depressurization rate, it is the largest that the various parts of the containment would experience during the blowdown. This rate can then be superimposed on the particulate layer to determine the condition for particle levitation.

Consider a particulate bed like that shown in Fig. 8.1 with height h and porosity ε. After an initial transient, the velocity of the gas as a function of height within the bed is given by Eq. (6.1), multiplied, of course, by the bed porosity ε. In particular, the gas velocity at the top of the bed is given by

$$u(h) = \frac{\varepsilon h}{P_o} \frac{dP}{dt} \tag{8.4}$$

The relaxation time to this quasi-steady-state result can be readily shown to be comparable to the time it takes an acoustic wave to span ("diffuse") the bed height, namely

$$t = \frac{h^2 \mu \varepsilon}{\kappa P_o} \tag{8.5}$$

where κ is the bed permeability and μ is the viscosity of the containment gas. For fission product particle beds composed of 10 μ particles and porosity ε = 0.4, the bed permeability is estimated to be 10^{-9} cm^2. Assuming P_o = 10 atm and a bed height of 1.0 cm, the relaxation time for attainment to quasi-steady conditions is 7×10^{-3} sec, which is completely negligible on the time scale of the containment blowdown.

Equation (8.4) can now be related to the Stokes velocity (U_s) for levitating individual particles

$$U_s = \frac{g(\rho_p - \rho)d^2}{18\,\mu} \tag{8.6}$$

where d is the particle diameter, and ρ_p is the particle density. Again using the above example, the velocity at the top of the bed is 1.3×10^{-5} m/s and the Stokes velocity for levitating individual particles is approximately 6 mm/sec, i.e. two orders of magnitude higher than the maximum throughput velocity. In this comparison, it must be remembered that the effective drag forces for a tightly packed bed can be substantially greater than the individual levitation velocity represented by the Stokes equation. In fact, this

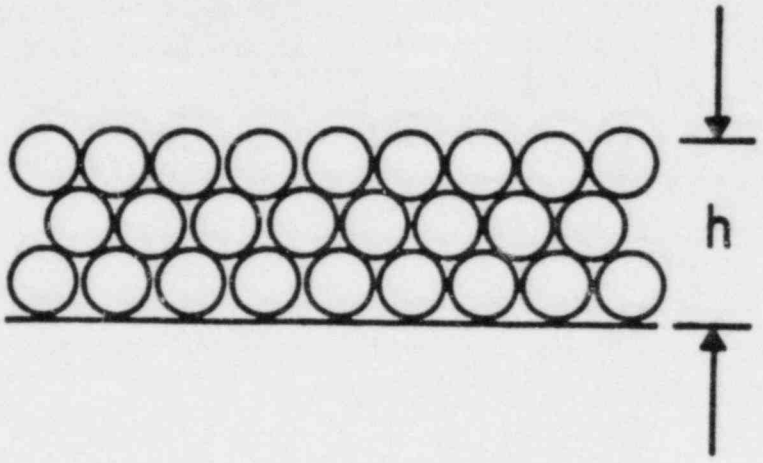

Fig. 8.1 Porous bed.

effective drag could be augmented almost 100 times. Therefore, the initial velocity for a very large break, such as 10 m^2 (far greater than that anticipated for containment failures), could potentially be sufficient to begin disrupting this particle layer (assumed to be 3 mm deep). However, as the bed loosens, this effective drag coefficient drops rapidly such that a porosity of about 90%, the multiplication factor on the effective drag coefficient is only about two. As a result, the velocities would be far below those required to support individual particles and the layer would collapse. Combining the above expressions, the relationship between the particle size levitated and the rupture size is given by

$$d = \left[\frac{18\ \mu\epsilon h n\ A_H \sqrt{RT}}{g(\rho_p - \rho)V}\right]^{1/2} \tag{8.9}$$

This expression can be compared to basic experiments in which the rupture size and particle layer depth can be varied independently.

8.3.2 Experimental Apparatus

These experiments were carried out in a cylindrical plexiglass test chamber closed on both ends by aluminum flanges. The chamber, which is shown in Fig. 8.2 had a diameter of 16.5 cm (6.5 in.) and a height of 61 cm (24 in.) providing a volume of approximately 0.013 m^3 (0.46 ft^3).

Simulated ruptures were at the top of this transparent chamber with the vent port being as large as 2.5 cm (1 in.) in diameter. The depressurization transient was measured through pressure taps in the upper flange and recorded on a Honeywell FM tape recorder. Particulate layers were created in either a shallow evaporating dish or a graduate placed at the bottom of the test chamber using either 10 micron nominal diameter glass beads. These layers varied from several millimeters to several centimeters deep to provide significant potential for particulate levitation to test the fundamental principles. The glass beads were dried and kept in sealed plastic bags to prevent moisture accumulation and coaggulation of the particles. In addition, lycopodium powder ($\sim$ 24 μm dia.) was mixed in with the 10 μm glass beads to

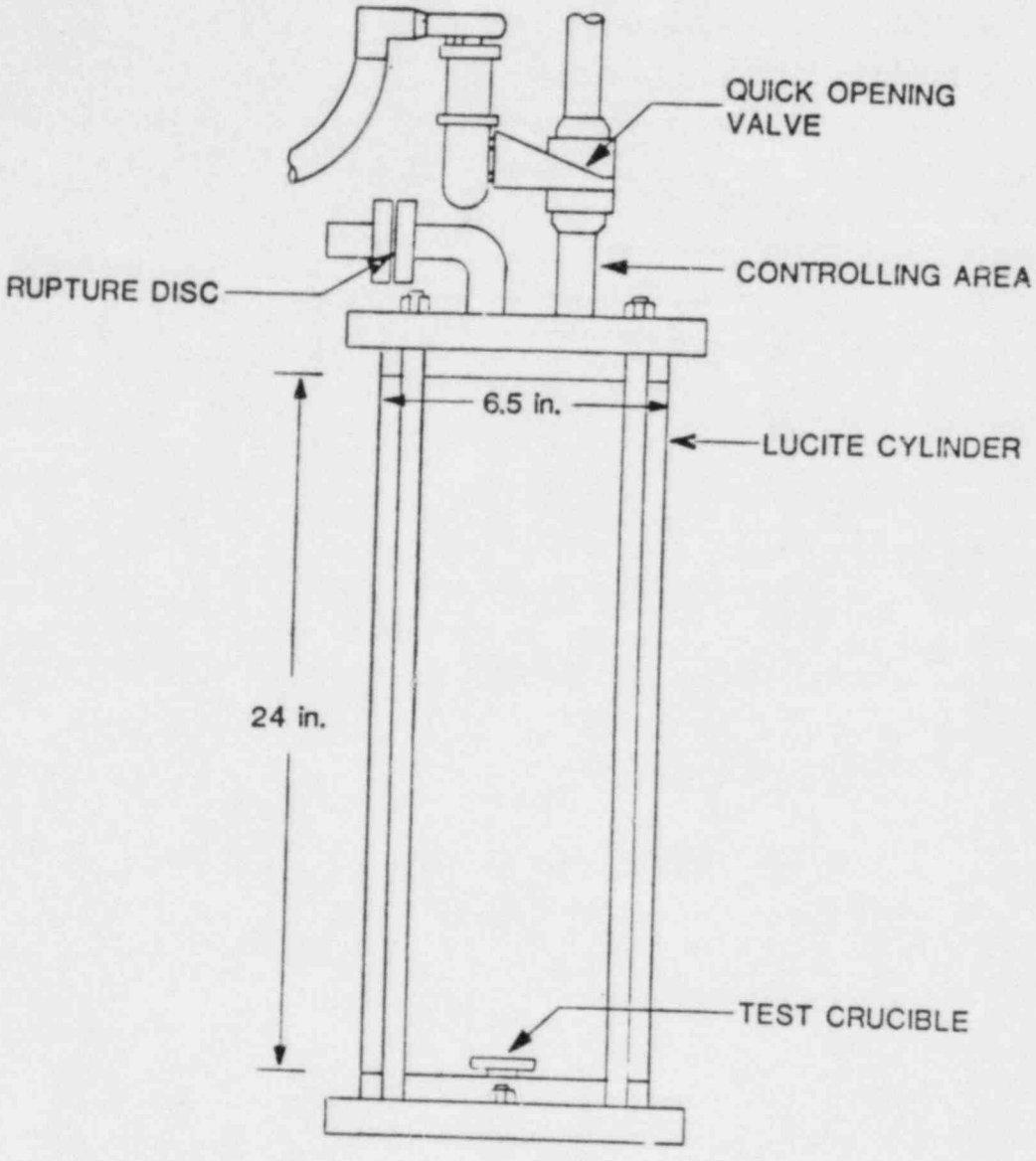

Fig. 8.2 Resuspension test vessel.

help prevent coaggulation. A typical mixture contained one-third lycopodium powder by volume. Also, the mixture was kept in sealed plastic bags to prevent moisture accumulation. Material levitation and removal was observed through two different observations, the first being video tape records of the experiments and the secord a weight loss measurement for the particulate layer as a result of the depressurization. This latter measurement was performed by weighing the sample before and after the experiment.

The entire apparatus is schematically represented in Fig. 8.3. Blowdown of the test vessel was through an air operated ball valve with the flow being limited by choked flow nozzle located just upstream of the valve. Exhaust gases were passed through a water pool and then through a fiber glass filter to remove any glass particulate.

Typical test conditions were blowdown from approximately 0.44 MPa (50 psig) at room temperature with particle layers varying from 2 mm to 11 cm. Nozzle diameters were varied from 2.5 cm (1 in.) down to 0.9 cm (0.36 in.).

8.3.3 Experimental Results

Measured vessel depressurization rates are compared with the isothermal predictions in Figs. 8.4 and 8.5. As illustrated, the simplified calculation adequately characterizes the data to determine the bed depressurization and thus the levitation potential.

The conditions tested in the experiments and the observations for each test are listed in Table 8.1. As shown, the material removal is a function of bed depth and nozzle diameter. Table 8.2 summarizes the experimental data in terms of the required bed depth to obtain debris dispersion for a given nozzle diameter. As shown, for the faster blowdowns where shallower beds could be used, the model predicts the required depth within a factor of two, i.e. sufficiently accurate to assess the potential for dispersion following containment failure. For deep beds, the material was lost from the test apparatus due to a single "cough" of the deep bed. As a result, material was pushed out of the graduate but immediately fell to the bottom of the test vessel. Hence, increased drag coefficient through a packed bed was sufficient

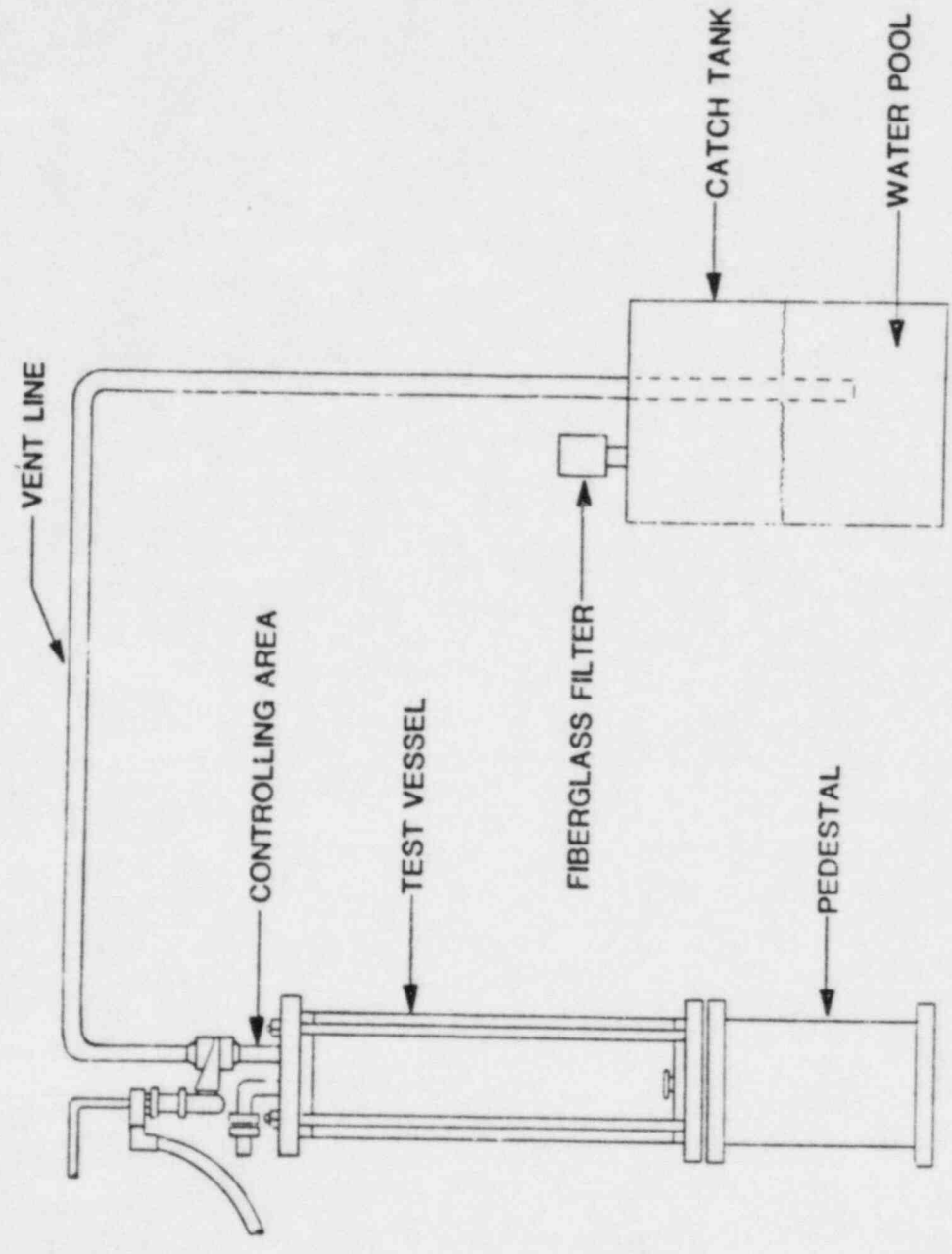

Fig. 8.3 Resuspension test apparatus.

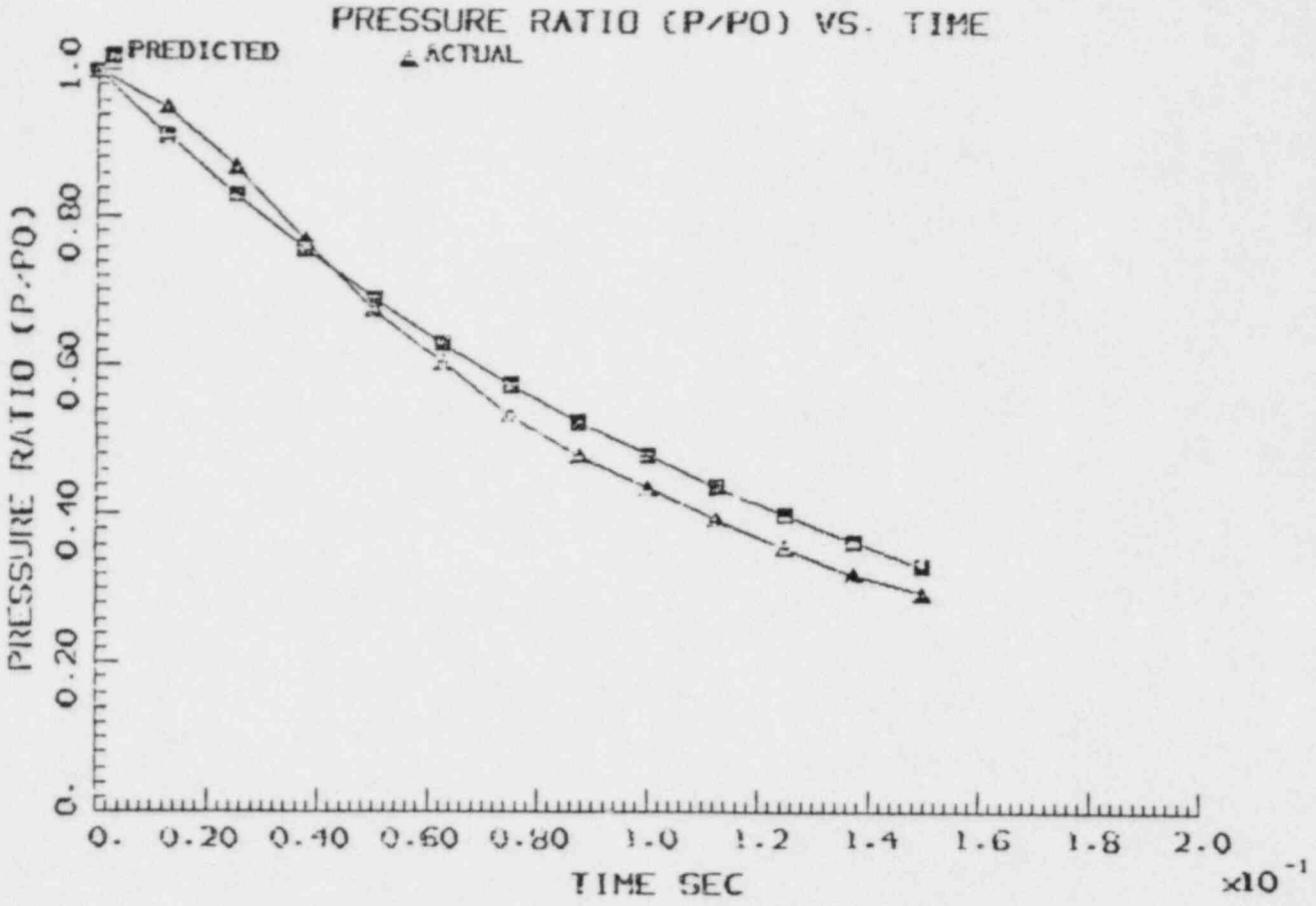

Fig. 8.4 Predicted and actual vessel pressure for P_o = 0.44 MPa and a nozzle diameter of 2.5 cm.

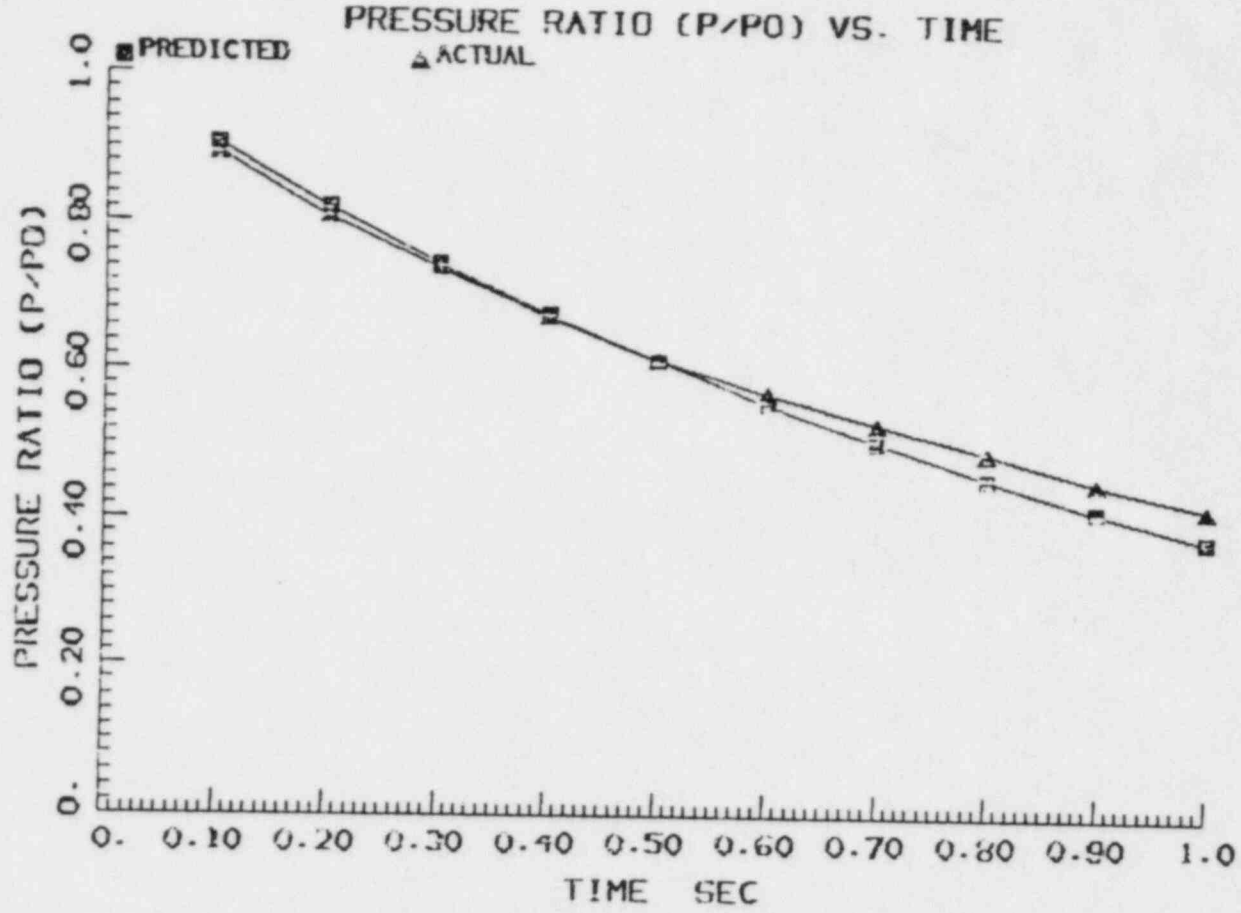

Fig. 8.5 Predicted and actual vessel pressure for P_o = 0.44 MPa and a nozzle diameter of 0.91 cm.

Table 8.1

RESUSPENSION TEST RESULTS

Run Number	Initial Pressure MPa	Nozzle Diameter (cm), in.	Bed* Depth cm	Material† Loss gm	Observation
1	0.44	2.54, 1		System Checkout	
2	0.44	2.5, 1	1	None	Slight Disturbance
3	0.44	2.5, 1	11	65.2	
4	0.44	2.5, 1	11	64.2	
5	0.44	2.5, 1	11	47	
6	0.44	2.5, 1	11	38	
7	0.44	2.5, 1	2	0.6	
8	0.44	2.5, 1	2	0.7	
9	0.44	2.5, 1	1	0.7	
10	0.44	0.91, 0.36	1	None	Slight Disturbance
11	0.44	0.91, 0.36	1	None	
12	0.44	0.91, 0.36	1	None	
13	0.44	0.91, 0.36	2	None	
14	0.44	0.91, 0.36	11	9	
15	0.44	0.91, 0.36		System Checkout	
16	0.44	0.91, 0.36	0.5	None	Very Slight
17	0.44 MPa	0.4, 0.180	1	None	
18	0.44 MPa	0.4, 0.180	1.6	None	Some Disturbance
19	0.44 MPa	0.4, 0.180	11	21	
20	0.62 MPa	0.4, 0.180	0.2	None	

*Average mass loading of the bed - 17.2 g/cm.

†Minimum detectable by weight measurement is 0.1 g.

Table 8.2

COMPARISON BETWEEN EXPERIMENTS AND RESUSPENSION MODEL

	Bed Depth Required to Resuspend Material	
Nozzle Diameter cm	Experimental cm	Predicted cm
2.5	1-2	2.7
0.91	11	21
0.46	11*	82

*Glass beads lost from the graduate were due to a single "cough" of the particle bed.

to cause the bed to open, but the glass beads were not suspended in the atmosphere. Consequently, the material was not resuspended by the depressurization.

In summary, experiments were carried out to demonstrate the relationship between depressurization and the potential for resuspension (dispersion) of settled material. The physical state of the deposited material is strongly influenced by its history on the sedimentation surface (wet or dry). A model was developed to predict the onset of resuspension for dry particulate layers. The model is in general agreement with the experimental results, in terms of characterizing the required layer thickness to initiate dispersion by depressurization. For thick beds, depressurization can cause the bed to "cough" or move as a slug. These very deep beds or layers, are not of interest for reactor systems and such movement does result in resuspension.

9.0 APPLICATION TO THE REACTOR ACCIDENTS

9.1 Primary System Evaluation

Fission products released from the fuel matrix, along with vapors of inert materials, as a result of extensive overheating would form a dense aerosol cloud as they flow out of the core region. Many of these particles, which could be solids and liquids, would agglomerate and deposit on surface structures in the upper plenum (PWRs) and separator (BWRs) region as well as other structures within the primary system. Depending upon the aerosol density, the specific configuration, their physical state, and the local power generation, particulate layers could be a few centimeters deep. Consequently, the potential for resuspension at the time of vessel failure should be assessed.

For PWR systems, the primary system volume is about 300 m^3 and the predicted breach sizes for failures beginning at the vessel penetrations is approximately 0.07 m^2. Assuming a debris depth of 5 cm and saturated steam at 15 MPa, Eq. (8.9) requires particle sizes smaller than 2 μm for dispersion. In such dense aerosol clouds, the particle sizes are generally much larger than this value. For example, the average particle sizes in Ref. [54] approach 10 μm for the aerosol concentrations of interest. Consequently, there would be little potential for dispersion of settled beds at the time of reactor vessel failure. Material accumulated on horizontal pipes (hot legs in particular) would likely be in such thin layers that the rapid blowdown through the breach would be too fast for the imposed velocity ($\sim$ 5 m/sec) to entrain significant material. However, some resuspension would be possible and should be evaluated.

Boiling water reactors have a volume of about 600 m^3 with a predicted breach size of approximately 0.13 m^2. Again assuming a debris depth of 5 cm and saturated steam at 7 MPa, Eq. (8.9) calculates a particle size of 2 μm or smaller. These particles are considerably less than would be anticipated for the dense aerosol cloud produced as fission products are released from the fuel. Consequently, dispersion of settled debris would not be significant. Also, BWRs have a more effective trapping geometry in the

separators than is the case for the PWR upper plenum and little horizontal surface for deposition and reentrainment, such as the PWR hot legs. In addition, BWRs are depressurized for the majority of the accident sequences considered. For these reasons, resuspension at the time of vessel failure would not be significant for BWR systems.

9.2 Containment Evaluation

Like the primary systems, the design of the specific containment and the accident sequence can have a substantial influence on the physical state of deposited material and thus on the potential for resuspension. For instance, pressure suppression (Mark I, Mark II, Mark III and ice condenser) designs can trap cesium iodide or cesium hydroxide in the suppression pool or in melted ice. This material would not be available for resuspension. Also, by virtue of the specific design, the Zion containment would have water on the containment floor for every accident sequence. Thus, aerosol material settled onto the floor would contact water, and in the case of cesium iodide and cesium hydroxide, enter into solution. As discussed in Section 8, this essentially eliminates and resuspension potential for these materials.

In addition to these design specific features, the particle size which would be resuspended from a dry bed of settled aerosols can be calculated using Eq. (8.9). The containment volumes for the IDCOR reference plants vary from 74,000 m^3 for Zion to about 12,500 m^3 for Peach Bottom. Containment failure locations and sizes where analyzed for Zion and reported in the Task 23.1 report [44]. This evaluation concluded that the regions for small penetrations (piping) were the most likely region for failure because of the numerous penetrations, the multiple failure modes and the complex interaction between the stretched containment wall and the anchored piping arrangement. These failures would result in areas from 0.01 m^2 to about 0.1 m^2 with the smallest being sufficient to terminate the pressurization. Other larger penetrations would be less likely to fail (require greater strain) and would create areas from 0.01 m^2 to 1 m^2. Lastly rupture of the containment shell was considered which could have a rupture area up to about 10 m^2. Using this largest area would provide an upper bound on the particle size that could be dispersed due to the depressurization.

For a large dry containment with the largest rupture area and a 1 cm deep bed of settled aerosol particles, Eq. (8.9) predicts an upper bound for dispersion of about 0.3 μm. This is much smaller than the sizes dominating the settling process. Consequently, even if the considerations of physical state are ignored, the potential for resuspension of a settled bed is insignificant.

The two most dominant accident sequences for Mark I systems fail the containment before the core is uncovered, thus dispersion at the time of containment failure is not an issue for these sequences. Nevertheless, Eq. (8.9) can be applied to the smaller volume system for the other accident sequences. Assuming the same large failure area (10 m^2) and the particle accumulation depth, the calculated size for resuspension by dispersion is 0.8 μm. This is also less than the sizes which dominate the sedimentation process, hence resuspension would not be a significant process in the Mark I either.

In summary, some resuspension could potentially occur during primary system blowdown for a PWR design but would not be significant for BWR designs. Evaluation of the spectrum of containment volumes represented by the IDCOR reference plants assuming a large containment failure size shows resuspension through dispersion of settled would not be a significant process.

10.0 CONCLUSIONS

In this report, the potential for resuspension of settled aerosols by tangential flows and dispersion of particle beds has been considered. These have assessed in light of available experimental results for tangential flows and basic experiments were carried out for depressurization cases. Several major conclusions can be made from this study.

- Thin layers of particulate held by electrostatic forces are so tightly bounded that even very high velocities would not strip them of the surface.

- Thicker particulate layers, like those that would be found on horizontal surfaces could be resuspended but only over long time intervals. Considering the blowdown character, either high velocities for short times or low velocities over long times, it can be concluded that resuspension throughout the containment volume would be insignificant even for large rupture sizes.

- Evaluation of potential debris accumulation in close proximity to localized penetration failures shows that the velocities over the top of the debris would be too small to resuspend the particles.

- Experiments on the physical state of cesium iodide and cesium hydroxide show that contact with water would essentially eliminate their potential for dispersion even if the water should eventually dryout.

- Experiments on debris dispersion show this phenomenon can be represented by simple physical models. These experiments also show that rapid depressurizations would be required to resuspend a debris accumulation and to maintain the suspended state.

- Extrapolation of the basic models to both BWR and PWR primary system designs show that some resuspension in the horizontal piping surfaces could possibly occur for a PWR but would not be anticipated for the BWR systems.

- Evaluation of the resuspension potential for the various containment designs considered in the IDCOR reference plant analyses shows that even if large rupture areas and dry particle beds are assumed, resuspension due to dispersion would be insignificant.

11.0 REFERENCES

1. F. P. Bowden and D. Tabor, The Friction and Lubrication of Solids, Oxford, Clarendon Press, 1950.
2. H. C. Hamaker, Physica, 4, 1058, 1937.
3. R. S. Bradley, Trans. Faraday Soc., 32, 1088, 1936.
4. B. V. Deryagin, Discuss. Faraday Soc., 18, 24, 1954.
5. A. P. Prosser and J. A. Kitchener, Nature, 178, 1339, 1956.
6. W. B. Kunkel, J. Appl. Phys., 21, 820, 1950.
7. T. G. Berg and N. Brunetz, Arch. Env. Health, 5. 26, 1962.
8. B. V. Deryagin and A. D. Zimon, Kolloid Zh. (Translation), 23, 454, 1961.
9. G. W. Penney and E. H. Klinger, AIEE Paper No. CP6/184, 1961.
10. M. Corn, J. Air Poll. Control Assoc., 11, 523, 1961.
11. M. J. Sparnaay, Nature, 108, 334, 1957.
12. J. G. Overbeek and M. Sparnaay, Discuss. Faraday Soc., 18, 12, 1954.
13. M. C. Kordecki and C. Orr, Arch. Env. Health, 1, 1, 1960.
14. M. Corn, J. Air Poll. Control Assoc., 11, 566, 1961.
15. G. Boehme, H. Krupp, H. Rabenhorst and G. Sandstede, Trans. Inst. Chem. Engrs. (London), 40, 18, 1962.
16. S. Bhattacharya and K. L. Mittal, Surf. Technology, 7, 413, 1978.
17. R. Polke, Bull. Soc. Chim. Fr., 9, 3241, 1969.
18. A. D. Zimon, "Adhesion of Dust and Powders," Plenum, 2nd edn., New York, 1981.
19. A. J. Raudviki, Loose Boundary Hydrodynamics, Pergamon, Oxford, 1967.
20. R. I. Larsen, Amer. Ind. Hyg. Assoc. J., 19, 265, 1958.
21. C. Orr, Jr. and J. M. Dallavalle, "Studies and Investigations of Agglomeration and Deagglomeration of Solid Particles," Report A-233, Georgia Institute of Technology, Engineering Experiment Station, Atlanta, 1956.
22. M. Corn and L. Silverman, Amer. Ind. Hyg. Assoc. J., 22, 337, 1961.

23. M. Corn and F. Stein, Amer. Ind. Hyg. Assoc. J., 26, 325, 1965.

24. A. J. Goldman, R. G. Cox and H. Brenner, Chem. Engng. Sci., 22, 653, 1967.

25. M. E. O'Neill, Chem. Engng. Sci., 23, 1293, 1968.

26. R. B. Bird, W. E. Stewart and E. N. Lightfoot, Transport Phenomena, John Wiley, New York, 1960.

27. F. Becker, Staub, 23, 60, 1963.

28. C. E. Lapple, J. Stasny and T. E. Wright, "High Velocity Filters," Tech. Rep. 55-457, Wright-Patterson Air Force Base, Ohio, A.S.T.I.A Document No. AD-142075, October 1957.

29. A. Fage and H. C. H. Townsend, Proc. Roy. Soc., Ser. A135, 656, 1932.

30. L. A. Masoroni and B. R. Fish, "Direct Observation of Particle Re-entrainment," Proc. Symp. Surface Contamination, Gothenburg, 1964.

31. S. J. Kline, W. C. Reynolds, F. A. Schraub and P. W. Runstadler, J. Fluid Mech., 30, 741, 1969.

32. E. R. Corino and S. J. Brodkey, J. Fluid Mech., 37, 1, 1969.

33. J. W. Cleaver and B. Yates, J. Colloid and Interface Sci, 44, 464, 1973.

34. S. K. Friedlander and H. F. Johnstone, Ind. Engng. Chem., 49, 1151, 1957.

35. G. A. Sehmel, J. Aerosol Sci., 4, 125, 1973.

36. R. A. Bagnold, The Physics of Wind Blown Sands and Desert Dunes, Methuen, London, 1941.

37. W. S. Chepil, Am. J. Sci., 255, 12, 1957.

38. W. S. Chepil and N. P. Woodruff, Am. J. Sci., 255, 104, 1957.

39. D. A. Gillette, I. H. Blifford, Jr. and C. R. Fenster, J. Appl. Meteorol., 11, 977, 1972.

40. G. A. Sehmel, "Tracer Particle Resuspension Caused by Wind Forces Upon an Asphalt Surface," Pacific Northwest Laboratories Annual Report for 1971 to USAEC/DBM, Vol. II: Physical Sciences, Part I: ATS, December 1972.

41. G. A. Sehmel and F. D. Lloyd, "Wind-Caused Particle Resuspension Rates," Pacific Northwest Laboratories Annual Report for 1976 to USERDA/DBER, BNWL-2100, Part 3, August 1977.

42. B. W. Reynolds and W. G. N. Slinn, "Experimental Studies of Resuspension and Weathering of Deposited Aerosol Particles," Oregon State University Report SR-0980-5 for USDOE, April 1979.

43. G. A. Sehmel, "Initial Correlation of Particle Resuspension Rates as a Function of Surface Roughness Height," Pacific Northwest Laboratories Annual Report for 1975 to USAEC/DBER, Part 3, ATS, February 1975.

44. M. M. Orgill, M. R. Peterson, and G. A. Sehmel, "Some Initial Measurements of DDT Resuspension and Translocation from Pacific NW Forests," Pacific Northwest Laboratories Annual Report for 1974 to USAEC/DBER, Part 3: ATS, February 1974.

45. "Zion Nuclear Generating Station, Integrated Containment Analysis," Technical Report on IDCOR Subtask 23.1, to be published.

46. "Sequoyah Nuclear Power Plant, Integrated Containment Analysis," Technical Report on IDCOR Subtask 23.1, to be published.

47. "Peach Bottom Atomic Power Station, Integrated Containment Analysis," Technical Report on IDCOR Task 23.1, to be published.

48. "Grand Gulf Nuclear Station, Integrated Containment Analysis," Technical Report on IDCOR Task 23.1, to be published.

49. "Containment Structural Capability of Light Water Nuclear Power Plants," IDCOR Technical Report on Subtask 10.1, July 1983.

50. B. Y. H. Liu and J. K. Agarwal, J. Aerosol Sci., 5, 145, 1974.

51. D. D. McCoy and T. J. Hanratty, Intl. J. Multiphase Flow, 3, 319, 1977.

52. "Debris Coolability, Vessel Penetration, and Debris Dispersal," IDCOR Technical Report on Subtask 15.2B, August 1983.

53. "Estimation of Fission Product and Core-Material Source Characteristics," Technical Report on IDCOR Subtasks 11.1, 11.4 and 11.5, October 1982.

54. N. A. Fuchs, The Mechanics of Aerosols, Pergamon Press, Oxford, 1964.

55. R. K. Hilliard, et al, "Results and Code Predictions for ABCOVE Aerosol Code Validation - Test AB5," HEDL-TME83-16, November 1983.

NRC Distribution:

R. Denning, BCL
M. Kuhlman, BCL
M. Lee, BCL
P. Cybulskis, Battelle
W. T. Pratt, BML
G. Greene
T. Ginsberg
H. Ludewig
T. Theofanous, Purdue
K. Winegardner, PNL
P. Owczarski, PNL
M. Berman, SNL
D. Powers, SNL
D. Dahlgren, SNL
R. Lipinski, SNL
K. Bergeron, SNL
J. Brochman, SNL
G. Weigand, SNL
S. Hodge, ORNL
T. Kress, ORNL
R. Wichner, ORNL
A. Wright, ORNL
R. Lorenz, ORNL
I. Catton, UCLA
M. Corradini, U. of Wisc.
J. Metcalf, Stone & Webster Eng.
P. MacDonald, EG&G-Idaho
R. Hobbins, EG&G
S. Levy, SNL
W. Castleman
A. Reynolds
W. Kastenberg
J. Cobble
L. Zumwalt

TECHNOLOGY for ENERGY CORPORATION

TO: Distribution

FROM: M. H. Fontana M H Fontana

DATE: August 2, 1984

SUBJECT: Transmittal Number 1 of Advance Material for IDCOR/NRC Meeting 3B.

Enclosed are copies of the following reports for the IDCOR/NRC Technical Exchange Meeting 3B -- Integrated Plant Analysis -- which will be held August 28-29, 1984, at the Rockville, MD., Holiday Inn Crowne Plaza:

(1) Grand Gulf Nuclear Station, IDCOR Task 23.1, Integrated Containment Analysis

(2) Evaluation of Containment Bypass and Failure to Isolate Sequences for the IDCOR Reference plants.

Remaining reports will be sent tomorrow.

/gf

IDO 884-004

ONE ENERGY CENTER PELLISSIPPI PARKWAY KNOXVILLE, TN 37922 PHONE (615) 966-5856 TELEX 810-570-1770

TECHNOLOGY for ENERGY CORPORATION

TO: Distribution

FROM: M. H. Fontana

DATE: August 2, 1984

SUBJECT: Transmittal Number 2 of Advance Material for IDCOR/NRC Meeting 3B.

Enclosed are copies of the following reports for the IDCOR/NRC Technical Exchange Meeting 3B -- Integrated Plant Analysis -- which will be held August 28-29, 1984, at the Rockville, MD., Holiday Inn Crowne Plaza:

(3) Peach Bottom Atomic Power Station, IDCOR Task 23.1, Integrated Analysis

(4) Zion Nuclear Generating Station, IDCOR Task 23.1, Integrated Containment Analysis.

The Sequoyah Report will be sent Monday.

/gf

IDO 884-004

ONE ENERGY CENTER PELLISSIPPI PARKWAY KNOXVILLE, TN 37922 PHONE (615) 966-5856 TELEX 810-570-1770